Variability in satellite winds over the Benguela upwelling system during 1999–2000

C. M. Risien,[1] C. J. C. Reason, and F. A. Shillington
Department of Oceanography, University of Cape Town, Rondebosch, South Africa

D. B. Chelton
College of Oceanic and Atmospheric Sciences, Oregon State University, Corvallis, Oregon, USA

Received 1 April 2003; revised 6 October 2003; accepted 25 November 2003; published 4 March 2004.

[1] Wind stress variability over the Benguela upwelling system is considered using 16 months (01 August 1999 to 29 November 2000) of satellite-derived QuikSCAT wind data. Variability is investigated using a type of artificial neural network, the self-organizing map (SOM), and a wavelet analysis. The SOM and wavelet analysis are applied to an extracted data set to find that the system may be divided into six discrete wind regimes. The wavelet power spectra for these wind regions span a range of frequencies from 4 to 64 days, with each region appearing to contain distinct periodicities. To the north, 10°–23.5°S, the majority of the power occurs during austral winter, with a 4–16 day periodicity. Further investigation of National Centers for Environmental Prediction reanalysis outgoing longwave radiation data indicates that the winter intensification of wind stress off the Angolan coast is linked with convective activity over equatorial West Africa. The summer activity appears to be linked with the intensification of the Angolan heat low. Convective activity over the Congo basin appears to impact upon wind stress variability, off the Angolan coast, throughout the year. Farther south, 24°–35°S, the majority of the power occurs in the summer. Here a bimodal distribution occurs, with peaks of 4–12 and 25–50 days. The southernmost regions appear to be forced at higher frequencies by both midlatitude cyclones (austral winter) and mesoscale coastal lows (austral summer). At lower frequencies, eastward propagating periodic wind events that originate over eastern South America appear to be important to the forcing of wind stress over the southern Benguela. *INDEX TERMS:* 4215 Oceanography: General: Climate and interannual variability (3309); 4247 Oceanography: General: Marine meteorology; 3360 Meteorology and Atmospheric Dynamics: Remote sensing; *KEYWORDS:* Benguela upwelling system, QuikSCAT satellite, wind stress variability

Citation: Risien, C. M., C. J. C. Reason, F. A. Shillington, and D. B. Chelton (2004), Variability in satellite winds over the Benguela upwelling system during 1999–2000, *J. Geophys. Res.*, *109*, C03010, doi:10.1029/2003JC001880.

1. Introduction

[2] The Benguela upwelling system, one of four major eastern boundary current regimes of the World Ocean [*Hill et al.*, 1998], is situated on the wide southwestern shelf of Africa, from Cape Agulhas (34.5°S) in the south [*Lutjeharms and Stockton*, 1987] to the Angolan-Benguela Front situated at approximately 14°–18°S in the north [*Shannon et al.*, 1987]. The Benguela system is unique among the four major upwelling systems of the world, in that it contains a warm-water boundary at both its most northern and southern extremities. Because of the fact that the tip of Africa extends only to 34.5°S, the Agulhas Current system is able to extend far enough westward that eddies and rings, shed by the current, are then able to interact with the southern boundary [*Gordon et al.*, 1987] as well as the offshore boundary [*Shillington et al.*, 1992] of the Benguela upwelling system.

[3] The Benguela upwelling system is strongly influenced by both the semi permanent high-pressure system over the subtropical South Atlantic, otherwise known as the South Atlantic Anticyclone (SAA), and the continental heat low that develops over southern Africa during the summer months. The prevailing winds in the region blow from a south to southeasterly direction. This in turn drives an offshore Ekman transport that results in the upwelling of cold, nutrient-rich water onto the continental shelf [*Peterson and Stramma*, 1991]. This upwelling exists with much spatial and temporal variability, all along the southwest coast of Africa, from Cape Agulhas to Cape Frio [*Lutjeharms and Meeuwis*, 1987]. Poleward of the Orange River (28.5°S), the dominant southeasterly wind regime is

[1]Now at College of Oceanic and Atmospheric Sciences, Oregon State University, Corvallis, Oregon, USA.

0148-0227/04/2003JC001880$09.00

modulated, by the passage of midlatitude cyclones south of the continent, and associated frontal systems. During the autumn months, the effect of this is usually seen in a weakening of the SAA and an abatement of southeasterly winds along the coast. During the winter months, however, westerly disturbances can, at times, result in gale force northwesterly and southwesterly winds. *Tyson and Preston-Whyte* [2000] suggest that this modulation occurs in cycles of 2–8 days.

[4] Other weather systems which occasionally modulate the upwelling favorable winds are cut off lows (spring and autumn), west coast troughs (summer), and coastal lows, mesoscale systems that are trapped by the coastal mountains and the subsidence inversion and which propagate as a type of Kelvin wave around the southern African coast [*Gill*, 1977; *Reason and Jury*, 1990]. Coastal lows tend to be forced by offshore flow trailing an eastward tracking anticyclone; this offshore flow, known locally as a berg wind, also has a significant impact on the upwelling region. In addition, local land-sea breezes [*Hart and Currie*, 1960] may be important in some locations, although usually the synoptic-scale wind masks their signature along the southern part of the west coast. The Benguela is particularly influenced by the diurnal pulsing of the local and regional winds while the entire region experiences seasonal variations of importance.

[5] Given the relatively complex meteorology of the region, and its oceanographic and economic significance via the upwelling, it is important to better understand the spatial and temporal variability of the coastal winds. The advent of satellite-derived winds now offers a unique opportunity to investigate this variability over the ocean away from coastal surface stations and other monitoring sites. Unlike the California upwelling system, there are very few meteorological buoys in the Benguela region so information from that potential source is extremely limited. Hence the objective of this paper is to analyze scatterometer winds obtained from the QuikSCAT satellite for the 1999–2000 period. Given the short time period of the data, but relatively high spatial resolution, we focus on the mesoseasonal to intraseasonal timescales and the spatial variability over the Benguela region. It should be noted that the period of analysis falls within the protracted 1998–2001 La Niña episode. Typically, high-pressure anomalies develop over the midlatitude South Atlantic and South Indian Oceans during La Niñas with low-pressure anomalies over southern Africa [*Reason et al.*, 2000], and hence stronger south easterlies tend to occur over the Benguela region (Figure 1). *Roy et al.* [2001] compared 1999–2000 austral summer conditions over the Benguela region with other La Niña events in the 1949–2000 period and determined that this particular summer was broadly similar to other events. Thus the analyses presented below must be viewed in the context of strong La Niña background forcing over the region.

2. Data and Methods

[6] The data analyzed herein are derived from the SeaWinds scatterometer, which was launched on 19 June 1999 onboard the QuikSCAT satellite. The SeaWinds instrument is an active microwave radar designed to measure the electromagnetic backscatter from the wind roughened ocean surface. This 16 month data record is analyzed from 01 August 1999 through to 29 November 2000. The u (offshore) and v (alongshore) wind stress components are sub sampled along a transect 200 km offshore from 10°–35°S from the QuikSCAT Level 3 data set. The data are smoothed temporally, to 2 day composites, and spatially, to a one-half-degree resolution, so as to significantly reduce the number of sampling errors within the data.

[7] Previous research, by authors such *Lutjeharms and Meeuwis* [1987], who used uncalibrated infrared Meteosat SST images to identify six localized upwelling regions, between the latitudes of 10 and 35°S, off the west coast of southern Africa (Figure 2), has shown that it is possible to divide the Benguela upwelling system into a number of biogeophysical provinces. In order to identify and classify distinct regions of wind stress within the Benguela upwelling system, a type of artificial neural network (ANN), which is particularly adept at pattern recognition and classification, is used. This ANN is known as the self-organizing map (SOM) [*Kohonen et al.*, 1995]. SOMs were first introduced to the climate community as part of a broader discussion on neural networks [*Hewitson and Crane*, 1994]. *Hewitson and Crane* [2002] related sea level pressure fields over the northeastern United States to station precipitation, while *Main* [1997] examined the seasonality of circulation in southern Africa, using both observed and GCM data. *Ainsworth* [1999] and *Ainsworth and Jones* [1999] used SOMs to improve chlorophyll estimates from satellite data through better pixel classification.

[8] Since SOMs are a relatively new technique, we describe the essentials of this analysis method below. The first step in the SOM procedure is to define a random distribution of nodes within a data space. Each of these nodes has an associated reference vector that is equal in dimension to the input vectors, i.e., input data. As the input vectors are presented to the SOM, the similarity between these vectors and each of the node vectors is calculated using Euclidean distances. The vector of the "winning" node is then modified, via the user defined learning rate, to reduce the difference between itself and the input vector. The input vectors are therefore simply used to adjust the location of the various SOM nodes in the data space. SOMs differ from most cluster algorithms in that, not only is the "winning" node updated but all of the surrounding nodes are also adjusted proportionally to their distance from that particular node. This iterative process continues until the changes in node location are negligible. The result is that the nodes will tend to cluster in regions of the data space that have higher data densities. The reference vectors are iteratively adjusted such that they span the data space with each node representing a position comparable to the median of the nearby data samples. The SOM is thus able to identify "arch-type" points, in the data space, which span the continuum of the data.

[9] SOMs have a number of advantages over more traditional statistical techniques. First, they are able to solve nonlinear problems of almost infinite complexity, and second, they tend to be more robust in the handling of noisy and missing data [*Dayhoff*, 1990]. For identifying groups in a data set, the primary advantage of SOMs is that the relationship among the identified nodes can be visualized in the same form as the original data. This can be an

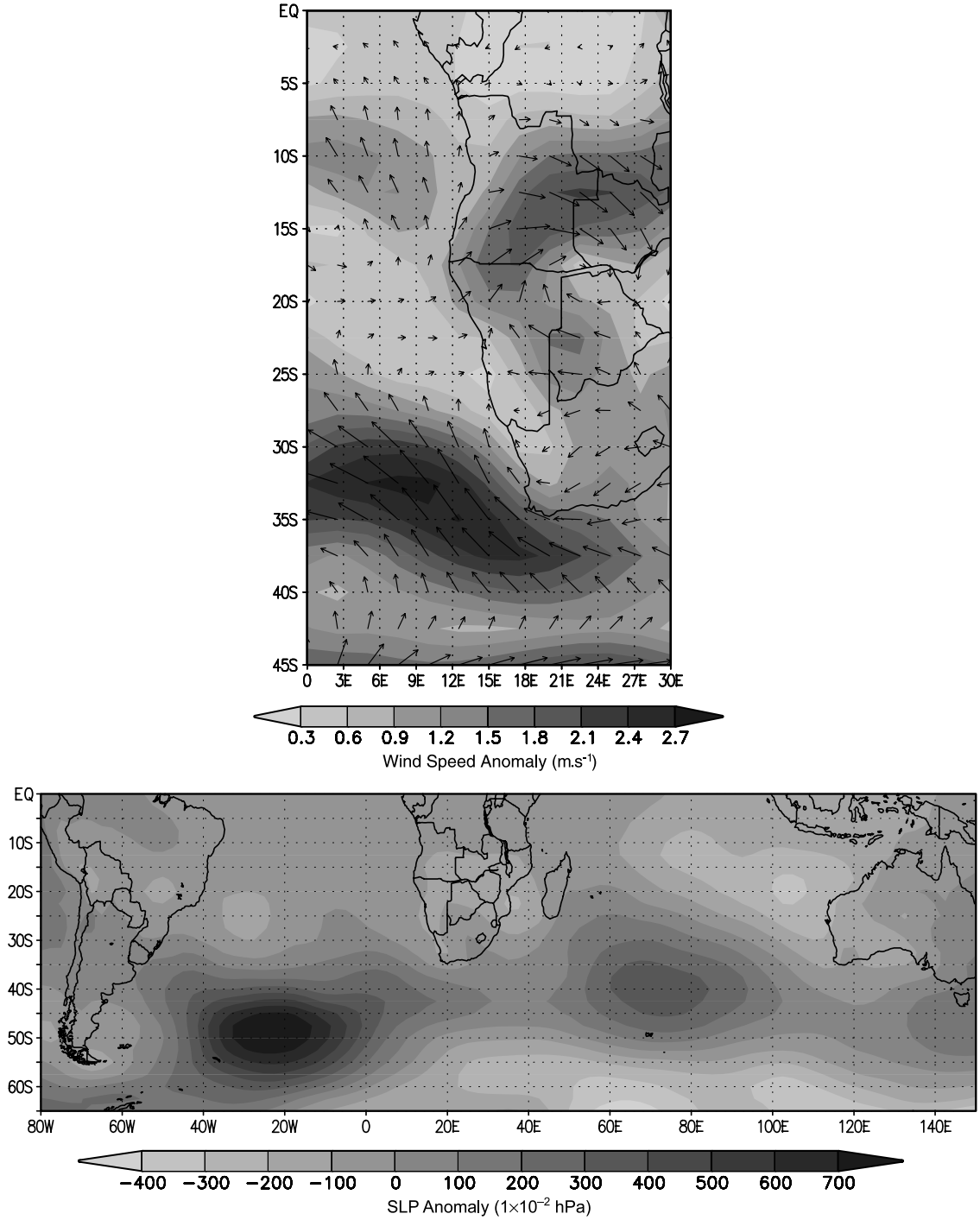

Figure 1. The composite anomaly (January–March 2000) of both wind, off the coast of southern Africa, and sea level pressure (SLP) over the South Indian/South Atlantic sectors of the Southern Hemisphere, as derived from the 2.5° resolution NCEP/NCAR reanalysis data set [*Kalnay et al.*, 1996]. The contour intervals are 0.3 m s^{-1} and 1 $\times$ 10^{-2} hPa, respectively.

advantage over other multivariate techniques such as cluster analysis, multidimensional scaling and principle component analysis (PCA), which yield various abstractions of the original data. As the output nodes duplicate the input format, SOMs are more easily interpreted than the outputs from other multivariate techniques.

[10] A perceived weakness to using SOMs is that there are no quantitative methods by which a researcher can choose the number of dimensions, represented by the SOM array. Assuming that the input data has an underlying continuum, the number of nodes chosen is dependent upon the level of detail required in the analysis. A large SOM array, i.e., many nodes, identifies a large number of patterns and in doing so reveals more detailed structure within the data, whereas a small SOM array identifies fewer, more generalized patterns. Thus the decision on the number of

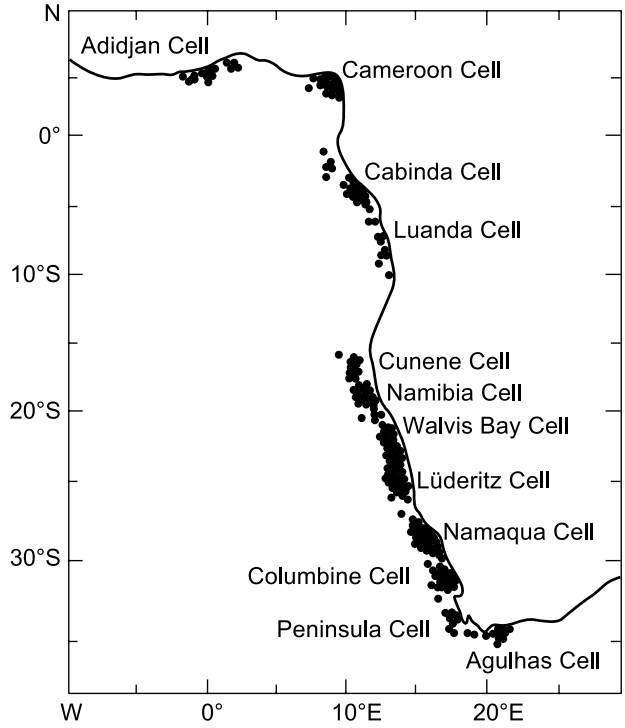

Figure 2. Distribution of the well-defined upwelling regions in the southeast Atlantic Ocean. Each dot represents the center of an upwelling event observed over a period of 156 weeks [after *Lutjeharms and Meeuwis*, 1987].

nodes in a SOM analysis is similar to that of the level of similarity required to identify groups in a cluster analysis. In this particular study, six nodes were chosen after some trial and error to assess the sensitivity of the results to both smaller and larger SOM arrays. For a more detailed review of the SOM methodology the reader is referred to *Hewitson and Crane* [2002] and *Kohonen et al.* [1995].

[11] For the SOM analysis, all u components are placed in the first half of the rows followed by all v components. The final input matrix consists of 488 columns (244 2 day composites $\times$ 2 components) $\times$ 51 rows (number of sampled latitudes). The analysis groups the data into six distinct wind regions that are associated with six respective time series (Figure 3), with each time series consisting of both a u and a v component.

[12] The v component time series is extracted for each of the six distinct wind regions, identified by the SOM analysis, and the periodicity of each of these time series is investigated using continuous wavelet analysis. Compared to Fourier analysis, wavelet analysis is a recently developed tool, which is well suited to the study of multiscale, nonstationary phenomena, occurring over finite spatial and temporal domains [*Lau and Weng*, 1995]. The continuous wavelet transform (CWT) has been used for various studies in meteorology and oceanography, including turbulence, surface gravity waves, low-level cold fronts, and variations in ENSO indicators such as the Southern Oscillation and Niño 3.4 SST. *Torrence and Compo* [1998] give a practical guide to wavelets, while the lectures by *Daubechies* [1992] provide readers with both an introductory and in-depth understanding of wavelets. The CWT allows for the decomposition of a signal $x[t]$ into fundamental contributions localized in time and frequency. This is done through the use of wavelets. These wavelets are obtained from a single function ψ by translations and dilations

$$\psi_{b,a}(\mathrm{t}) = \frac{1}{a}\psi\left(\frac{t-b}{a}\right), \tag{1}$$

where $a > 0$ is the dilatation parameter and b is the time translation parameter. The CWT expands the time series $x[t]$ into a two-dimensional parameter space $[b, a]$ and yields a measure of relative amplitude of local activity (over an interval proportional to a) at scale a and time b [*Mélice et al.*, 2001]. The choice of wavelet ψ depends on the signal to be analyzed. For this investigation the Morlet wavelet was chosen. This wavelet is one of the most widely used wavelets in geophysics [*Lau and Weng*, 1995]. The Morlet wavelet is a complex cosine wave modulated by a Gaussian function

$$\psi(t) = \pi^{1/4} e^{-t^2/2} e^{i\omega_0 t}, \tag{2}$$

with $i = [-1]^{1/2}$ and where $\omega_0 = \pi\,[2/\ln 2]^{1/2}$ [*Daubechies*, 1992] is chosen to be large enough to ensure that $\psi[t]$ satisfies the admissibility condition which practically is equivalent to

$$\int_{-\infty}^{\infty} \psi(t)\, dt = 0. \tag{3}$$

As the Morlet wavelet is complex, the wavelet transform coefficient $W[b, a]$ is also complex and may be expressed in terms of real and imaginary parts, modulus and phase.

[13] By inverting the scale of the Morlet wavelet, the CWT becomes a time frequency analysis where the dilatation parameter a corresponds to the period and the translation parameter b corresponds to the time. In equation (1), the normalization $1/a$ is used instead of the usual $1/[a]^{1/2}$. With this normalization, the components of the CWT may be directly compared to each other and the Morlet wavelet can be interpreted as a band-pass linear filter of weight $1/a$ centered around $\omega = \omega_0/a$. This filter allows the extraction of the different local components of the signal such as its local value, amplitude and phase, for each point of the $[b, a]$ time frequency space [*Mélice et al.*, 2001].

3. Results and Discussion

[14] The global climatic context of 1999–2000 was characterized by a pronounced La Niña event that strengthened in DJF 2000 after weakening earlier in 1999. The results, presented below, should thus be regarded with caution when comparing them to the climatological average.

3.1. SOM Analysis

[15] Figure 3 characterizes the time series for each of the six distinct wind regions identified via the SOM analysis. Region 1 (10°–15°S) is dominated by light southwesterly wind stress throughout the study period (01 August 1999 to 29 November 2000), with an average wind stress of approximately 0.03 N m^{-2}. Figure 3 indicates pulses of stronger winds during the April–October 2000 period.

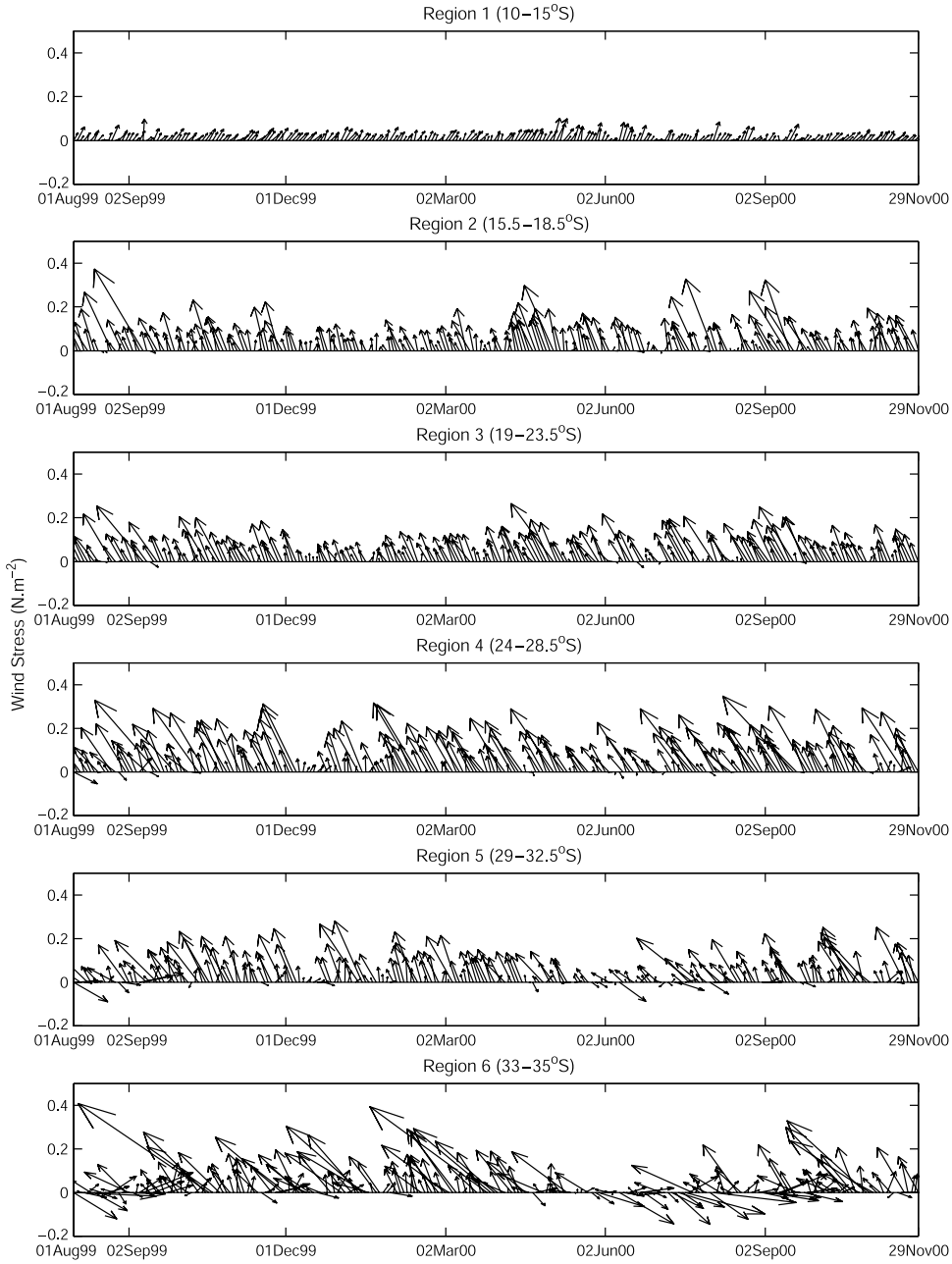

Figure 3. Feather plots of each of the six distinct wind regions (10°–15°, 15.5°–18.5°, 19°–23.5°, 24°–28.5°, 29°–32.5°, and 33°–35°S) as identified via the SOM analysis (01 August 1999 to 29 November 2000).

Given that during the boreal summer, the tropical southeastern Atlantic is a source region for moisture feeding into the Congo basin and the West African monsoon region, these pulses may reflect fluctuations in tropical convective activity here. The evidence for this suggestion is discussed below.

[16] Region 2 (15.5°–18°S) is more representative of the wind stress experienced over the Benguela upwelling regime. These winds exhibit strong and consistent south-southeasterly components, with an average wind stress of about 0.1 N m^{-2}. Winds are generally weakest in austral summer when the South Atlantic anticyclone is furthest south and there is convergence into the Angola low [*Mulenga*, 1999]. In addition to a general strengthening during austral winter half of the year, there are shorter periods of more intense winds, again perhaps reflecting pulsing in the convective regions over the Congo basin and West Africa and their inflows from the tropical SE Atlantic. The most substantial peak in wind stress occurs at the beginning of May 2000, where wind stresses of 0.2 N m^{-2} are recorded.

[17] Region 3 (19°–23.5°S) exhibits a similar wind stress pattern to that of region 2, with the wind stress retaining a south-southeasterly component throughout the study period. Again, an average wind stress value of approximately 0.1 N m^{-2} is recorded. The period of intensified wind

stress, which generally occurs from April 2000 through to October 2000 in regions 1 and 2, is also evident in region 3. This maximum is however, marginally weaker and less pronounced.

[18] Region 4 (24°–28.5°S) contains three periods of relatively strong wind stress (>0.2 N m^{-2}). The first period extends from the beginning of the time series, 01 August 1999, to roughly early December 1999. A second period starts a month or so later and continues to about early May 2000, while the third period again lasts approximately five months from mid-June 2000 through to the end of November 2000. Separating these maxima are two shorter periods of relatively low wind stress (~0.05 N m^{-2}) lasting for approximately one month each. Also noticable in region 4 is the larger mean wind stress (reflecting the mean position of the South Atlantic Anticyclone) and larger synoptic variability, relative to region 3. This increase in synoptic variability may be due to the fact that region 4 is affected to a greater degree than region 3 by both migrating anticyclones and westerly disturbances passing south of South Africa and by troughs in the easterly flow across low-latitude southern Africa. These tropical and midlatitude features therefore modulate the coastal pressure gradient, and hence the winds, on synoptic timescales [*Tyson and Preston-Whyte*, 2000].

[19] To the south lies a domain that stretches from 29°S to 32.5°S, region 5. Here, wind reversals, i.e., northwesterly winds, become noticable with the occasional intrusion of the westerly wind belt during the winter months. These events are however, relatively infrequent and wind stress with a south-southeasterly component still dominates. This region contains reduced wind stress for the months of May, June, and July 2000. A maximum in stress occurs in mid-October 1999. No such maximum occurs during October 2000.

[20] Region 6 (33°–35°S) is the southernmost region and, as such, exhibits the highest degree of synoptic wind stress variability since migratory anticyclones and frontal systems directly influence it. This particular region contains five distinct periods. The first period extends from approximately the beginning of August to mid-October 2000. This period is dominated by relatively weak southwesterly wind stress. Following this, is a lengthy summer period from mid-October 1999 to mid-May 2000, dominated by anticyclonic conditions with relatively strong southeasterly wind stress (>0.1 N m^{-2}). Weak westerly to northwesterly winds, associated with the northerly migration of the westerly wind belt during winter, occur during mid-May through to the end of July 2000. The beginning of August 2000 brings with it, once again, light southerly to southwesterly wind stress as the SAA starts to ridge farther south in spring. This period lasts until approximately the end of September when stronger anticyclonic conditions begin once more. The final period, dominated by relatively strong southeasterly wind stress, extends from the beginning of October to the end of November 2000.

3.2. Wavelet Analysis

[21] The wavelet power spectra, presented below, span a range of frequencies with periods from approximately 4–64 days. The exact form of these spectral peaks is partly governed by the wavelet "uncertainty principal" [*Chui*, 1992] that precludes the possibility of achieving high localisation in time and frequency simultaneously, and thus depends somewhat on the choice of the wavelet function. That said, the event-like, sporadic, and pulsating nature of the variability within the Benguela upwelling system is one attribute of these data that stands out. Periods of high variability are well resolved and tend to appear as isolated peaks. The occurrence and duration of these spectral peaks is, however, somewhat irregular, and strongly dependent on latitude.

[22] The spectral peaks in wind stress for the two northernmost regions differ greatly from those situated farther south, with region 3 appearing as an area of transition between the tropical regions to the north (Figures 4–5) and the subtropical regions to the south (Figures 6–9). To the north (Figures 4–5), the maximum in wind stress energy occurs from the beginning of May to the end of September, during which the variability is dominated by periods ranging from 4 to 16 days. The integrated spectral diagram (Figure 4c) indicates a maximum at a 10 day period for region 1. Farther south this peak shifts to somewhat shorter periods, with regions 2 and 3 containing peaks at 7–8 days respectively (Figures 5c and 6c). Region 2 also contains a relatively weaker ~40 day peak. This peak extends throughout the latter part of 1999 before waning and reappearing again in mid-February 2000 (Figure 5b). It continues to be evident throughout most of 2000 with stronger energy near the onset and cessation date of the West African monsoon (i.e., early May and September). Region 1 shows no such peak, however.

[23] A wavelet analysis of region 1's *u* component time series (not shown) reveals spectral peaks at approximately 4, 10, 20, and 45 days. The 4 and 10 day peaks correspond well with the wavelet analysis of outgoing longwave radiation (OLR) over the Congo basin for the same time period (not shown). To investigate possible links between the northern Benguela wind stress and convection centers over the nearby land, Figure 10 presents two wavelet analyses of National Centers for Environmental Prediction (NCEP) reanalysis OLR data [*Liebmann and Smith*, 1996] during the period 01 August 1999 to 29 November 2000 for the West African region (12.5°N, 10°E; Figure 10a) and the Angolan region (15°S, 15°E; Figure 10b). The OLR wavelet transforms show that, in both cases, almost all of the spectral energy occurs during the summer when tropical convection intensifies (note that Angola lies in the Southern Hemisphere and West Africa in the northern). Angola's integrated spectral diagram shows peaks at approximately 8, 14, and 40 days. The West African integrated spectral diagram depicts a broad peak of 4–10 days, as well as a peak of lesser amplitude at approximately 30 days. As mentioned above, the *v* component time series for region 1 shows no spectral peak of approximately 40 days. The *u* component does, however, contain a ~40 day spectral peak similar to that of the OLR peak over Angola. This manifestation of the low-frequency peak in the *u* rather than the *v* component may in part be due to the fact that tropical zonal winds appear to incorporate more energy at the lower frequencies than do meridional winds [*Burpee*, 1972], and that north of about 15°S, the coastal winds show a significant easterly or onshore component feeding into convection over Angola and the Congo basin.

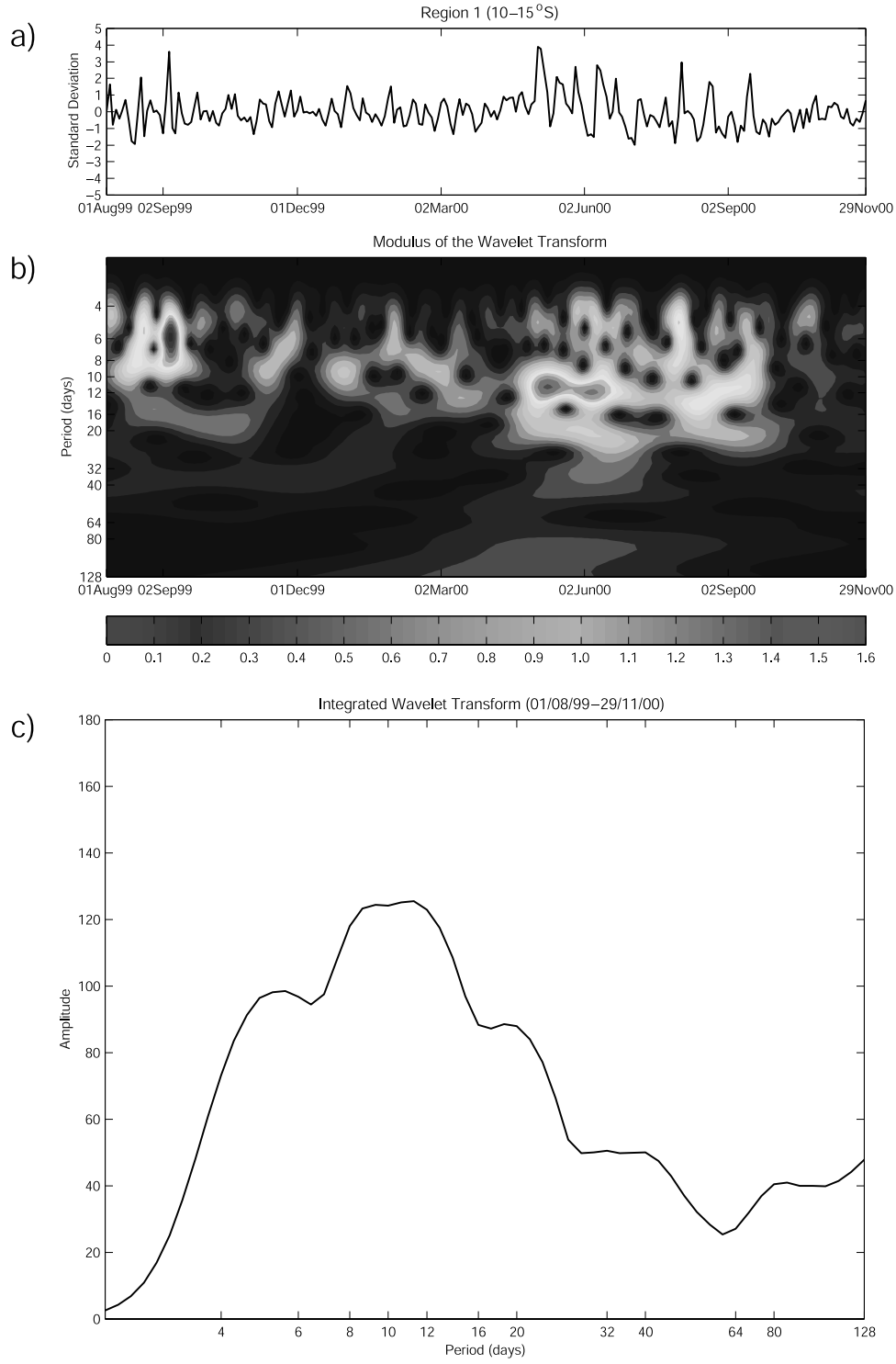

Figure 4. Region 1 (10°–15°S). (a) The standardized time series of the alongshore (v) component winds (01 August 1999 to 29 November 2000), (b) the modulus of the wavelet transform, using the Morlet wavelet, and (c) the integrated wavelet transform. The contour interval in Figure 4b is 0.1. See color version of this figure at back of this issue.

[24] It thus appears that the wind stress variability observed in regions 1 and 2 can be explained, in part, as resulting from a combination of at least two factors: first, the seasonal shift in the SAA, and second, the convective activity associated with the Angola low, West African monsoon, and the Congo basin. Another possible source of intraseasonal variability is the so-called Madden-Julian Oscillation (MJO). *Madden and Julian* [1971, 1972] originally identified MJOs to be a 40–50 day tropical oscillation. It is beyond the scope of this study to determine

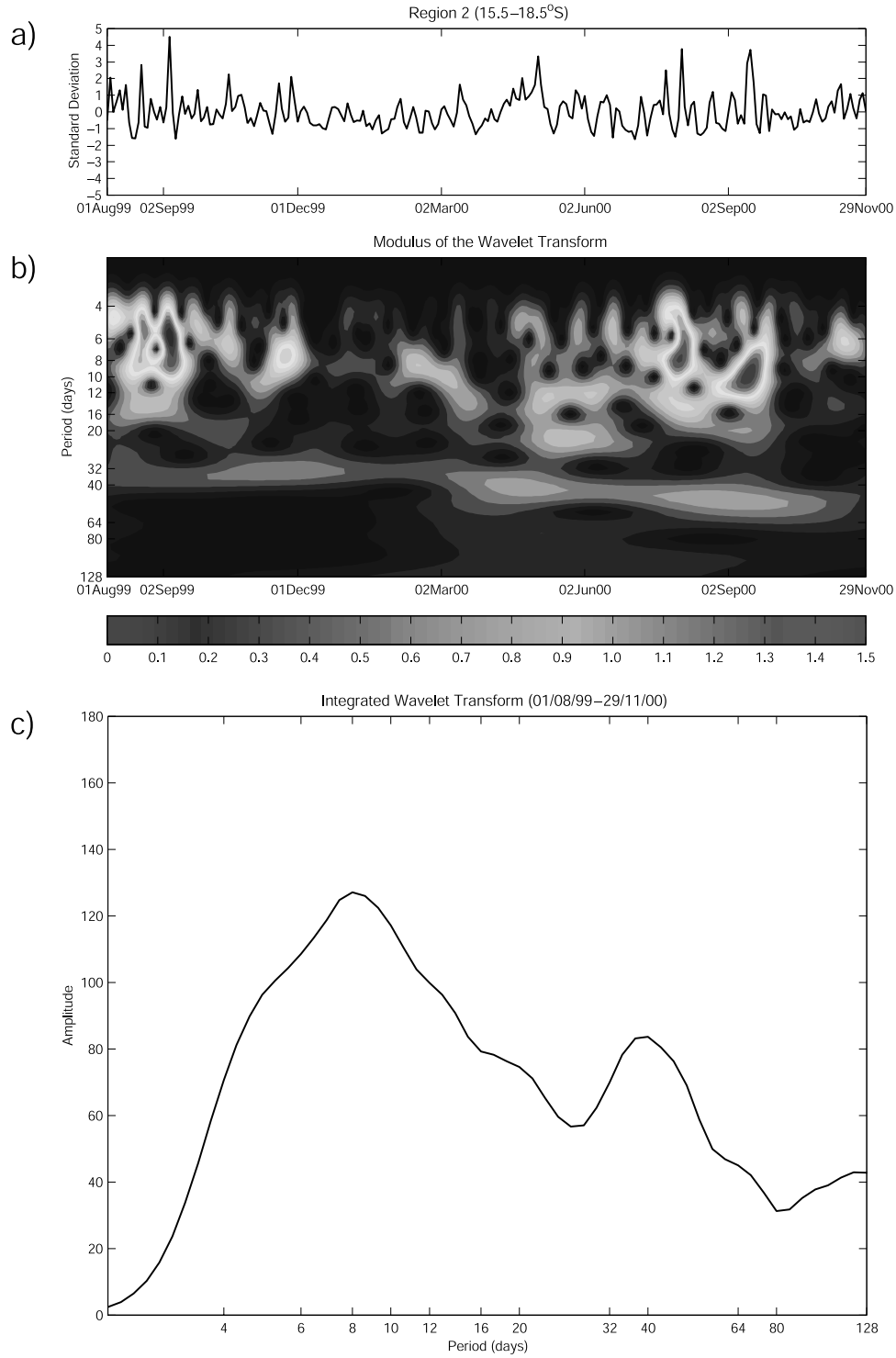

Figure 5. Region 2 (15.5°–18.5°S). (a) The standardized time series of the alongshore (v) component winds (01 August 1999 to 29 November 2000), (b) the modulus of the wavelet transform, using the Morlet wavelet, and (c) the integrated wavelet transform. The contour interval in Figure 5b is 0.1. See color version of this figure at back of this issue.

whether MJOs are contributing significantly to the wind variability in regions 1 and 2; however, we note that *Madden and Julian* [1994] more recently described MJOs to be relatively broadband phenomena with a central frequency that is not fixed but varies in time.

[25] Farther south there is evidence of approximately 25–50 day variability that is centred around 40 days. This variability becomes increasingly apparent toward the mid-latitudes (compare Figures 6–9). Region 3 (Figure 6) at 19°–23.5°S again appears to be a transition zone between

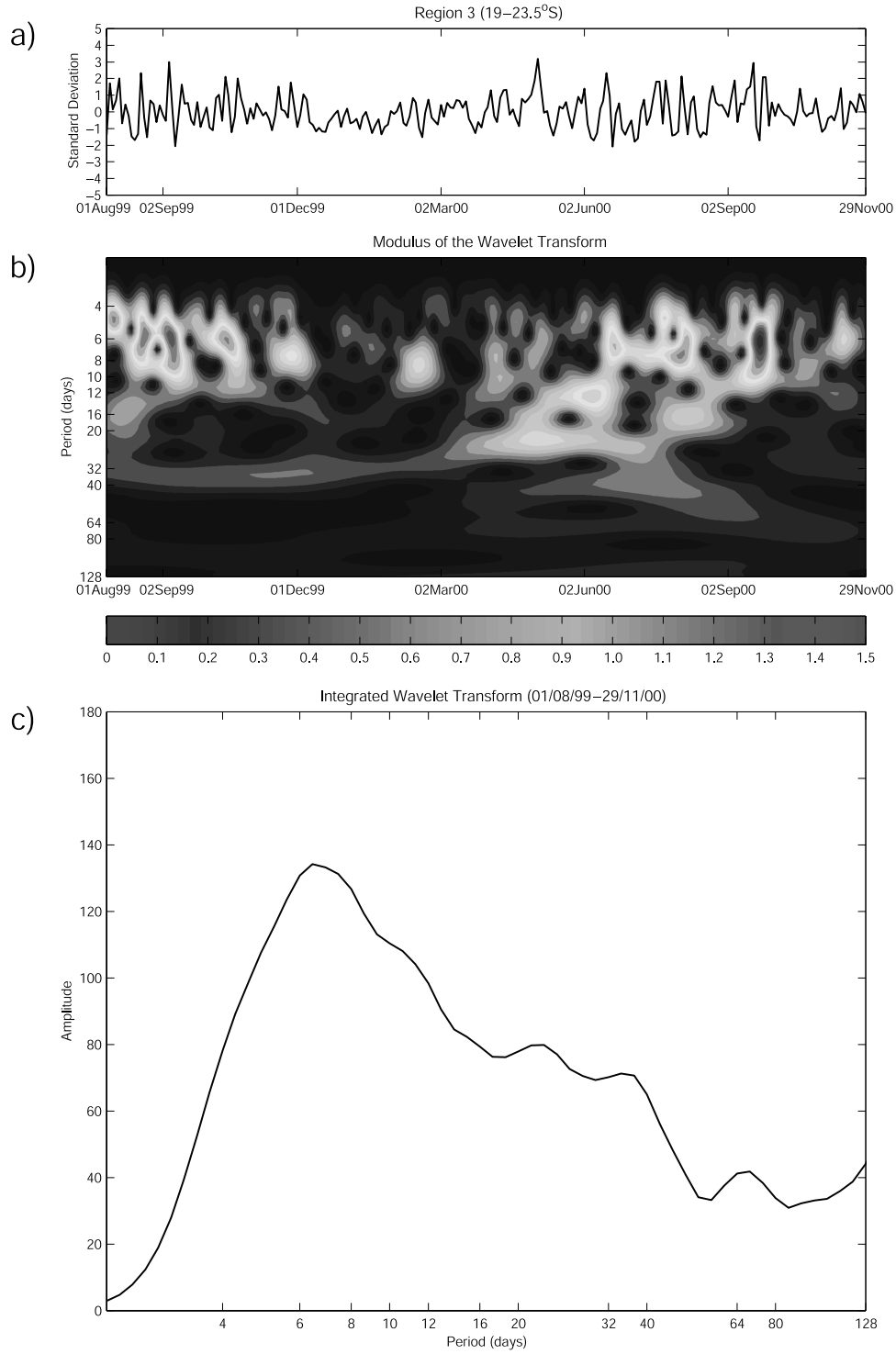

Figure 6. Region 3 (19°–23.5°S). (a) The standardized time series of the alongshore (v) component winds (01 August 1999 to 29 November 2000), (b) the modulus of the wavelet transform, using the Morlet wavelet, and (c) the integrated wavelet transform. The contour interval in Figure 6b is 0.1. See color version of this figure at back of this issue.

the tropical and subtropical regions and shows little evidence of energy between 25 and 50 days. The 40 day centered peak is visible for much of the study period in regions 4–6. Variability in this 40 day band has two relative maxima. These maxima occur in all three of these southern regions, and last for at least 3–4 months. The first peak occurs between October and February 1999, while the second peak occurs from September 2000 onward (Figures 7–9b). One possible source of such intraseasonal variability, in these subtropical to midlatitude regions, is via the nonlinear interaction of the mean westerly flow aloft with the Andes Cordillera [*Dickey et al.*, 1991; *Marcus et*

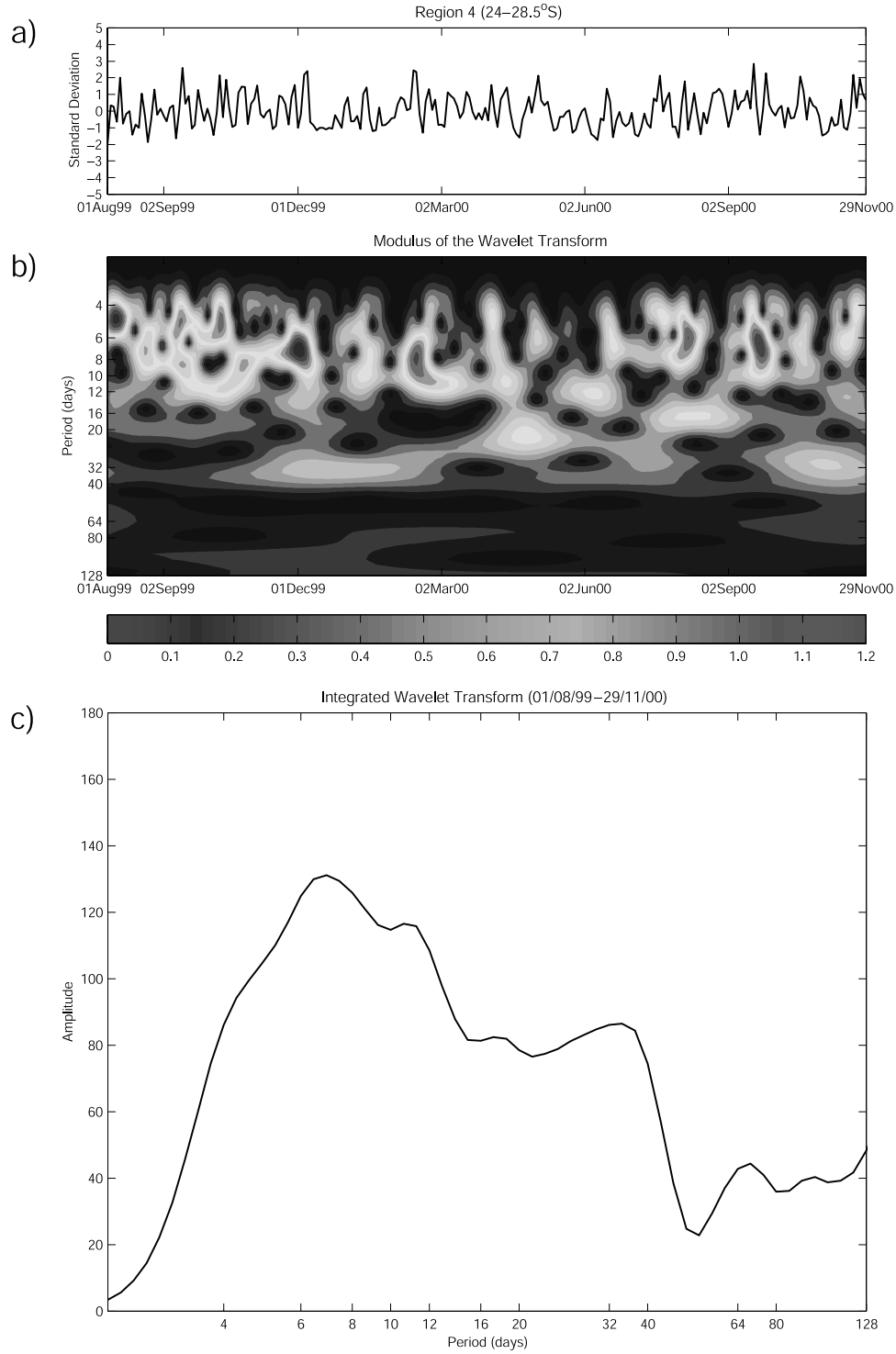

Figure 7. Region 4 (24°–28.5°S). (a) The standardized time series of the alongshore (v) component winds (01 August 1999 to 29 November 2000), (b) the modulus of the wavelet transform, using the Morlet wavelet, and (c) the integrated wavelet transform. The contour interval in Figure 7b is 0.1. See color version of this figure at back of this issue.

al., 1994]. Further analysis of QuikSCAT data (Figure 11) shows that this variability appears to result from quasi-periodic wind events, which originate over eastern South America and then propagate eastward across the South Atlantic with a phase speed of approximately 250 km d^{-1}.

[26] On quasi-synoptic scales, regions 3, 4, 5, and 6 all contain a band of frequencies ranging from 4–12 days (Figures 6–9). This broad peak, which includes the synoptic cycle of around 2–8 days [*Tyson and Preston-Whyte*, 2000], has greater amplitude in regions 3 and 4 than farther south.

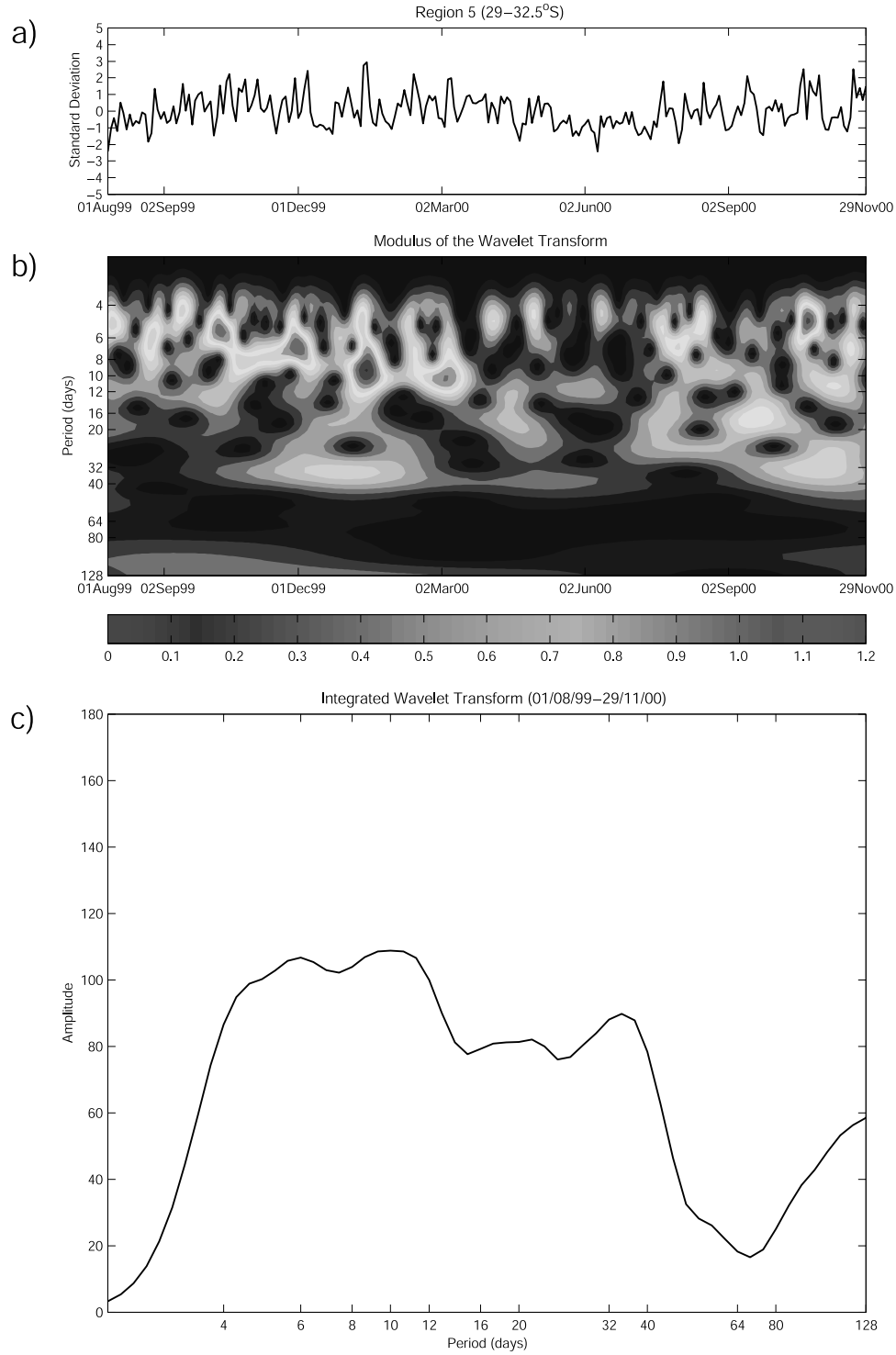

Figure 8. Region 5 (29°–32.5°S). (a) The standardized time series of the alongshore (v) component winds (01 August 1999 to 29 November 2000), (b) the modulus of the wavelet transform, using the Morlet wavelet, and (c) the integrated wavelet transform. The contour interval in Figure 8b is 0.1. See color version of this figure at back of this issue.

Previous analyses of sea level pressure and sea level data [*Kamstra*, 1987; *Preston-Whyte and Tyson*, 1973; *Hunter*, 1987; *Jury et al.*, 1990], have all found similar short-period (4–12 day) fluctuations off the coast of southern Africa. The broader quasi-synoptic peaks in the southernmost regions likely reflect the greater range of transient weather systems experienced in the southern Benguela. In addition to fronts, these include cut off lows, mesoscale coastally trapped lows, and west coast troughs, none of which have a significant signature north of about 23°S.

[27] Regions 4–6, show less seasonal variability in synoptic and similar timescale activity than the northern regions

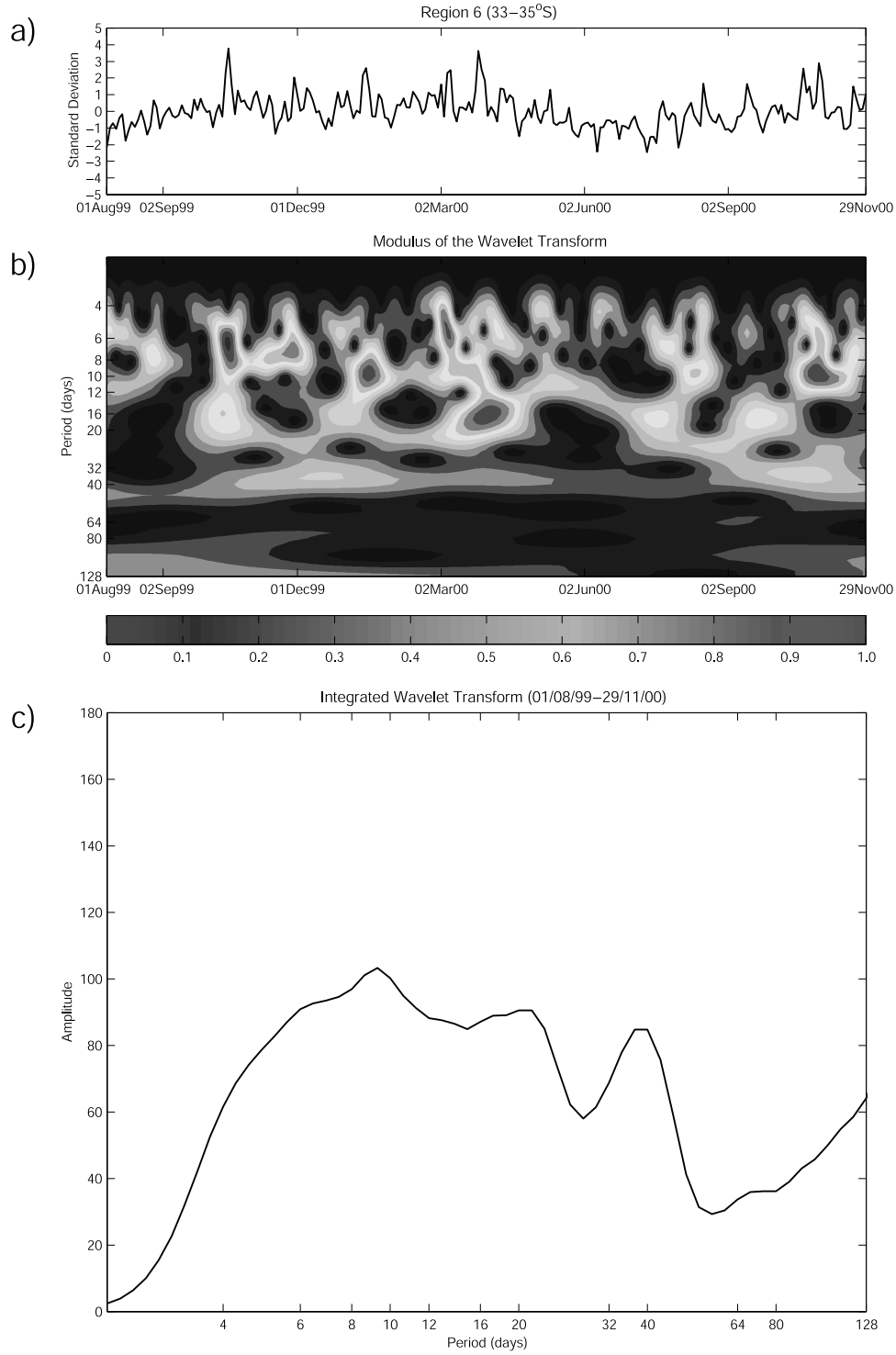

Figure 9. Region 6 (33°–35°S). (a) The standardized time series of the alongshore (v) component winds (01 August 1999 to 29 November 2000), (b) the modulus of the wavelet transform, using the Morlet wavelet, and (c) the integrated wavelet transform. The contour interval in Figure 9b is 0.1. See color version of this figure at back of this issue.

where the majority of the spectral peaks occur between late austral autumn and early spring, i.e., during the West African monsoon season. However, a brief reduction in the intensity of wind stress events in the three southernmost regions does appear to occur for April through to mid-July. For the most part, however, a major event occurs approximately once every 40 days. The lack of seasonal variability in near-synoptic-scale activity for the three southernmost regions reflects the influence of midlatitude Rossby wave activity throughout the year and the relatively small sea-

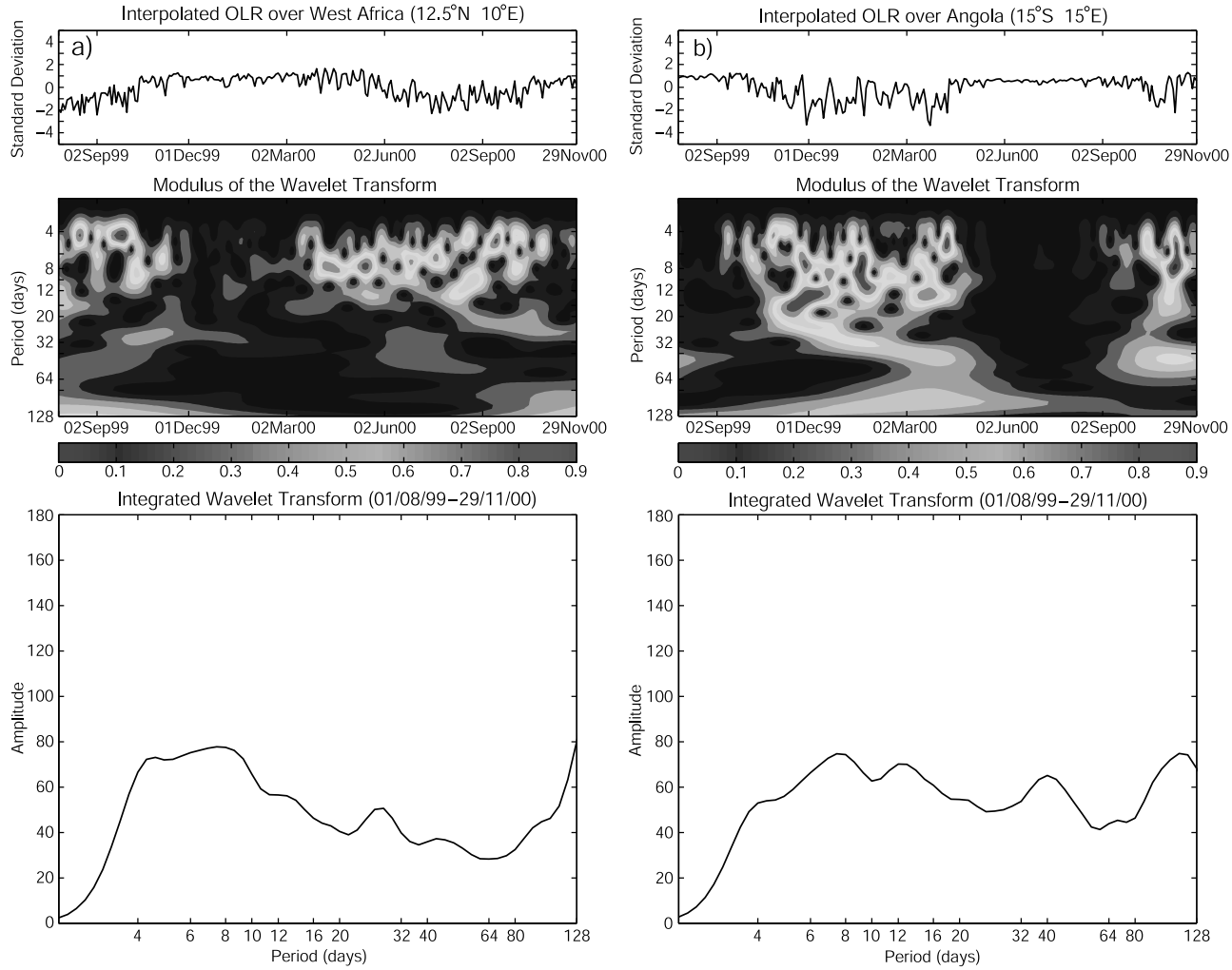

Figure 10. (a) The standardized time series of interpolated OLR data, as derived from the 2.5° resolution NCEP reanalysis data set [*Liebmann and Smith*, 1996], the modulus of the wavelet transform, using the Morlet wavelet, and the integrated wavelet transform for 12.5°N, 10°E (01 August 1999 to 29 November 2000). (b) As above but for 15°S, 15°E. The contour interval, for both Figures 10a and 10b, is 0.1. See color version of this figure at back of this issue.

sonal shift in the central latitude of the SAA [*Tyson and Preston-Whyte*, 2000]. As a result of Africa terminating at relatively low latitude (34.5°S), the SAA only shifts about 5°–6° of latitude between winter and summer, considerably less than the NE Pacific and Azores highs. Significant synoptic-scale pulsing of the coastal wind over the southern Benguela thus occurs throughout the year, although this pulsing may be more obviously frontal in nature during winter and more likely as mesoscale coastal lows or west coast troughs during summer (depending on the strength and height of the subsidence inversion relative to the coastal mountains) [*Reason*, 1996; *Tyson and Preston-Whyte*, 2000].

4. Conclusions

[28] This study applied a Kohonen (SOM) and wavelet analysis to examine regional wind stress variability over the Benguela upwelling system using 16 months of satellite-derived QuikSCAT wind data. The SOM analysis suggests that the Benguela system may be divided into six discrete wind regions (10°–15°S; 15.5°–18.5°S; 19°–23.5°S; 24°–28.5°S; 29°–32.5°S; and 33°–35°S). The wavelet power spectra for each of these regions span a range of frequencies from 4–64 days. The intermittent and pulsating nature of the Benguela system was highlighted through the wavelet analysis. Areas of high variability were well resolved and tended to appear as isolated peaks. The occurrence and duration of these peaks was, however, found to be somewhat irregular, and strongly latitude dependent. North of 23.5°S, the majority of the power occurred during the austral winter, with a 6–16 day periodicity. The analyses suggest that this winter intensification off the Angolan coast is linked to convective activity over West Africa. The summer activity is more likely a result of the intensification of the Angolan low, which is a center of convection over tropical southern Africa. Equatorial convective activity over the Congo basin appears to have an impact upon wind stress variability throughout the year.

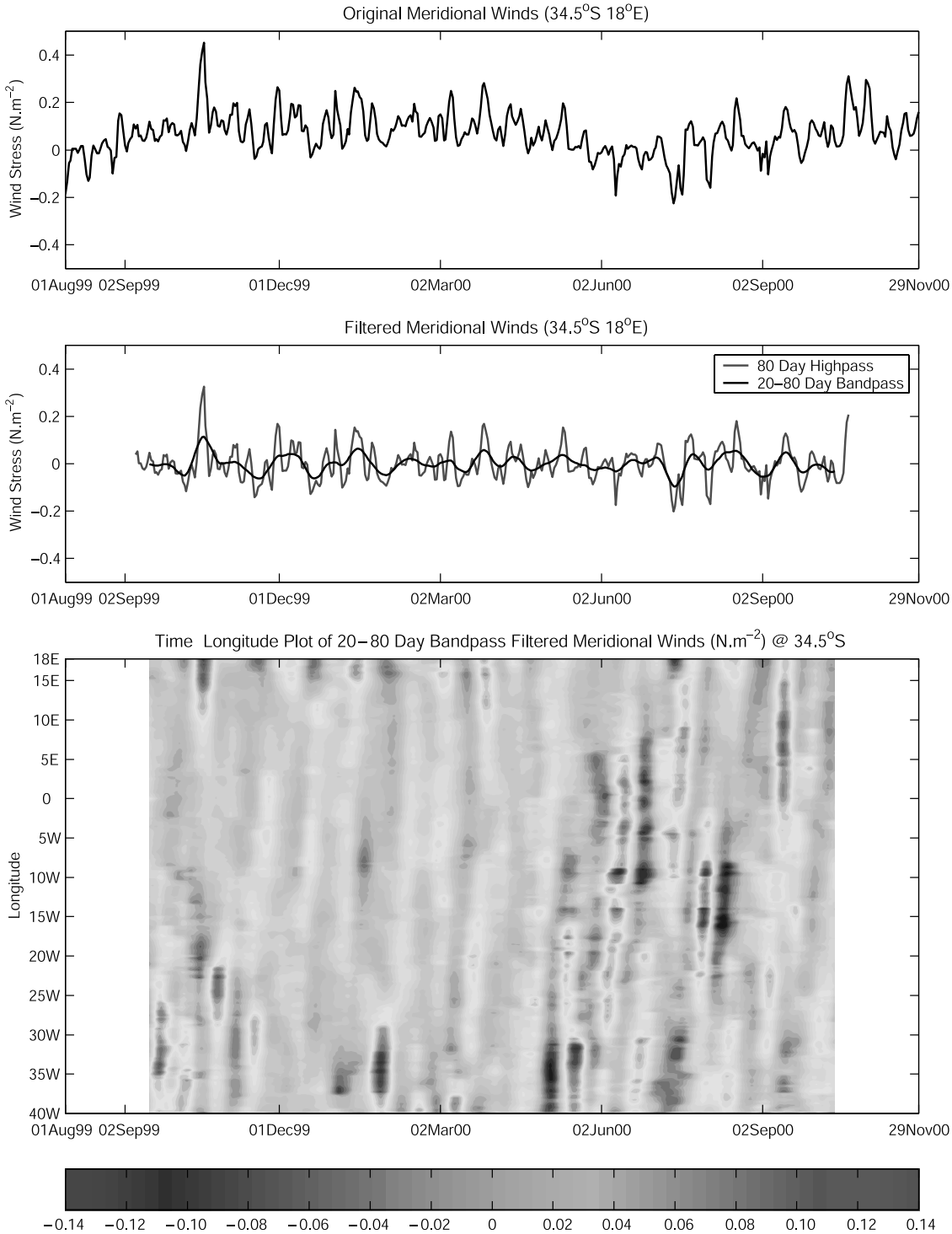

Figure 11. (top) The original QuikSCAT meridional wind stress time series (01 August 1999 to 29 November 2000) at 34.5°S, 18°E. (middle) The high-pass- (80 day) and band-pass- (20–80 day) filtered time series (10 September 1999 to 21 October 2000 and 18 September 1999 to 13 October 2000, respectively). (bottom) A time (18 September 1999 to 13 October 2000)-longitude (40°W–18°E) plot of 20–80 day band-pass-filtered meridional winds at 34.5°S. The contour interval for Figure 11 (bottom) is 0.02 N m^{-2}. See color version of this figure at back of this issue.

[29] South of 24°S, the majority of the power occurred during the summer months. Within this region, a bimodal distribution was found to occur with peaks of 4–12 days and 25–50 days, respectively. The southernmost regions appear to be forced by midlatitude cyclones during the austral winter and by mesoscale coastal lows during the austral summer. At lower frequencies, wind events that originate off the southeast coast of South America and

propagate eastward across the South Atlantic with a phase speed of approximately 250 km.d^{-1} are suggested to be important to the forcing of ~40 day wind stress variability over the southern Benguela upwelling system.

[30] This work provides further understanding of the synoptic to intraseasonal-scale variability in the winds over the Benguela upwelling system. As mentioned above, the Benguela upwelling system is extremely important to the countries of southern Africa both in terms of its fish stocks and mineral wealth (diamonds, natural gas, and oil). In order to make use of these resources in a sustainable and responsible fashion, it is crucial to obtain a better understanding of the system's atmospheric forcing and its associated impacts on parameters such as upwelling rates, nutrient supply and shelf-open ocean exchanges. A new multidisciplinary and multinational project is commencing shortly to investigate in detail the impacts of this atmospheric forcing on the shelf circulation and biota off the west coast of southern Africa.

[31] **Acknowledgments.** This research forms part of the first author's MSc, completed at the University of Cape Town, and partial funding thereof by the NRF and DACST is gratefully acknowledged. DBC was supported by NASA grant NAS5-32965 for funding of Ocean Vector Winds Science Team activities. Jean-Luc Mélice is thanked for providing the original wavelet analysis MATLAB code. Two anonymous reviewers provided helpful comments, which significantly improved the manuscript. Last the authors would like to thank Anthony Richardson and Eric Maloney for helpful discussions.

References

Ainsworth, E. J. (1999), Visualization of ocean colour and temperature from multispectral imagery captured by the Japanese ADEOS satellite, *J. Visualization*, *2*, 195–204.

Ainsworth, E. J., and S. F. Jones (1999), Radiance spectra classification from the ocean color and temperature scanner on ADEOS, *IEEE Trans. Geosci. Remote Sensing*, *37*, 1645–1656.

Burpee, R. W. (1972), The origin and structure of easterly waves in the lower troposphere of North Africa, *J. Atmos. Sci.*, *29*, 77–90.

Chui, C. K. (1992), *An Introduction to Wavelets*, 266 pp., Academic, San Diego, Calif.

Daubechies, I. (1992), *Ten Lectures on Wavelets*, 357 pp., Soc. for Ind. and Appl. Math., Philadelphia, Pa.

Dayhoff, J. E. (1990), *Neural Network Architectures: An Introduction*, 259 pp., Van Nostrand Reinhold, New York.

Dickey, J. O., M. Ghil, and S. L. Marcus (1991), Extratropical aspects of the 40–50 oscillation in the length-of-day and atmospheric angular momentum, *J. Geophys. Res.*, *96*, 2643–2658.

Gill, A. E. (1977), Coastally trapped waves in the atmosphere, *Q. J. R. Meteorol. Soc.*, *103*, 431–440.

Gordon, A. L., J. R. E. Lutjeharms, and M. L. Gründlingh (1987), Stratification and circulation at the Agulhas retroflection, *Deep Sea Res., Part A*, *34*, 565–599.

Hart, T. J., and R. I. Currie (1960), The Benguela Current, *Discovery Rep.*, *31*, 123–298.

Hewitson, B. C., and R. G. Crane (1994), *Neural Nets: Applications in Geography*, Kluwer Acad., Norwell, Mass.

Hewitson, B. C., and R. G. Crane (2002), Self-organizing maps: Applications to synoptic climatology, *Clim. Res.*, *22*, 13–26.

Hill, A. E., B. M. Hickey, F. A. Shillington, P. T. Strub, K. H. Brink, E. D. Barton, and A. C. Thomas (1998), Eastern ocean boundaries coastal segment (E), in *The Sea*, vol. 11, edited by A. R. Robinson and K. H. Brink, chap. 2, pp. 29–67, John Wiley, Hoboken, N. J.

Hunter, I. T. (1987), Weather of the Agulhas Bank and the Cape south coast, unpublished M.S. diss, Univ. of Cape Town, Cape Town, South Africa.

Jury, M. R., C. MacArthur, and G. B. Brundrit (1990), Pulsing of the Benguela upwelling region: Large-scale atmospheric controls, *S. Afr. J. Mar. Sci.*, *9*, 27–41.

Kalnay, E., et al. (1996), The NCEP/NCAR 40-year reanalysis project, *Bull. Am. Meteorol. Soc.*, *77*, 437–471.

Kamstra, F. (1987), Interannual variability in the spectra of the daily surface pressure at four stations in the Southern Hemisphere, *Tellus, Ser. A*, *39*, 509–514.

Kohonen, T., J. Hynninen, J. Kangas, and J. Laaksonen (1995), The self-organizing map program package, version 3.1., Helsinki Univ. of Technol., Helsinki, Finland. (Available at http://www.cis.hut.fi/research/som-research/nnrc-programs.shtml.)

Lau, K.-M., and H.-Y. Weng (1995), Climate signal detection using wavelet transform: How to make a time series sing, *Bull. Am. Meteorol. Soc.*, *76*, 61–78.

Liebmann, B., and C. A. Smith (1996), Description of a complete [interpolated] outgoing longwave radiation dataset, *Bull. Am. Meteorol. Soc.*, *77*, 1275–1277.

Lutjeharms, J. R. E., and J. M. Meeuwis (1987), The extent and variability of south-east Atlantic upwelling, in *The Benguela and Comparable Ecosystems*, edited by A. I. L. Payne, J. A. Gulland, and K. H. Brink, *S. Afr. J. Mar. Sci.*, *5*, 51–62.

Lutjeharms, J. R. E., and P. L. Stockton (1987), Kinematics of the upwelling front off southern Africa, in *The Benguela and Comparable Ecosystems*, edited by A. I. L. Payne, J. A. Gulland, and K. H. Brink, *S. Afr. J. Mar. Sci.*, *5*, 25–49.

Madden, R. A., and P. Julian (1971), Detection of a 40–50 day oscillation in the zonal wind, *J. Atmos. Sci.*, *28*, 702–708.

Madden, R. A., and P. Julian (1972), Description of global-scale circulation Regions in the Tropics with a 40–50 period, *J Atmos. Sci.*, *29*, 1109–1123.

Madden, R. A., and P. Julian (1994), Observations of the 40–50 day tropical oscillation—A review, *Mon. Weather Rev.*, *122*, 814–837.

Main, J. P. L. (1997), Seasonality of circulation in southern Africa using the Kohonen Self-Organising Map, M.S. diss., Univ. of Cape Town, Cape Town, South Africa.

Marcus, S. L., M. Ghil, and J. O. Dickey (1994), The extratropical 40-day oscillation in the UCLA General Circulation Model. Part 1: Atmospheric momentum, *J. Atmos. Sci.*, *51*, 1431–1446.

Mélice, J. L., A. Coron, and A. Berger (2001), Amplitude and frequency modulation of the Earth's obliquity for the last million years, *J. Clim.*, *14*, 1043–1054.

Mulenga, H. M. (1999), Southern African climate anomalies, summer rainfall and the Angola low, Ph.D. diss., Univ. of Cape Town, Cape Town, South Africa.

Peterson, R. G., and L. Stramma (1991), Upper-level circulation in the South Atlantic Ocean, *Prog. Oceanogr.*, *26*, 1–73.

Preston-Whyte, R. A., and P. D. Tyson (1973), Note on pressure oscillations over South Africa, *Mon. Weather Rev.*, *101*, 650–653.

Reason, C. J. C. (1996), Topography and the dynamical response to easterly flow in Southern Hemisphere subtropical west coast regions, *Meteorol. Atmos. Phys.*, *61*, 187–199.

Reason, C. J. C., and M. R. Jury (1990), On the generation and propagation of the southern African coastal low, *Q. J. R. Meteorol. Soc.*, *116*, 1133–1151.

Reason, C. J. C., R. J. Allan, J. A. Lindesay, and T. J. Ansell (2000), ENSO and climatic signals across the Indian Ocean Basin in the global context: Part 1, Interannual composite patterns, *Int. J. Climatol.*, *20*, 1285–1327.

Roy, C., S. Weeks, M. Rouault, G. Nelson, R. Barlow, and C. van der Lingen (2001), Extreme oceanographic events recorded in the southern Benguela during the 1999–2000 summer season, *S. Afr. J. Sci.*, *97*, 465–471.

Shannon, L. V., J. J. Agenbag, and M. E. L. Buys (1987), Large- and mesoscale features of the Angola-Benguela Front, in *The Benguela and Comparable Ecosystems*, edited by A. I. L. Payne, J. A. Gulland, and K. H. Brink, *S. Afr. J. Mar. Sci.*, *5*, 11–24.

Shillington, F. A., L. Hutchings, T. A. Probyn, H. N. Waldron, and W. T. Peterson (1992), Filaments and the Benguela Frontal zone: Offshore advection or recirculating loops?, in *Benguela Trophic Functioning*, edited by A. I. L. Payne et al., *S. Afr. J. Mar. Sci.*, *12*, 207–218.

Torrence, C., and G. P. Compo (1998), A practical guide to wavelet analysis, *Bull. Am. Meteorol. Soc.*, *79*, 61–78.

Tyson, P. D., and R. A. Preston-Whyte (2000), *The Weather and Climate of Southern Africa*, Oxford Univ. Press, New York.

D. B. Chelton and C. M. Risien, College of Oceanic and Atmospheric Sciences, Oregon State University, 104 COAS Administration Building, Corvallis, OR 97331-5503, USA. (crisien@coas.oregonstate.edu)

C. J. C. Reason and F. A. Shillington, Department of Oceanography, University of Cape Town, Private Bag, Rondebosch, 7701, South Africa.

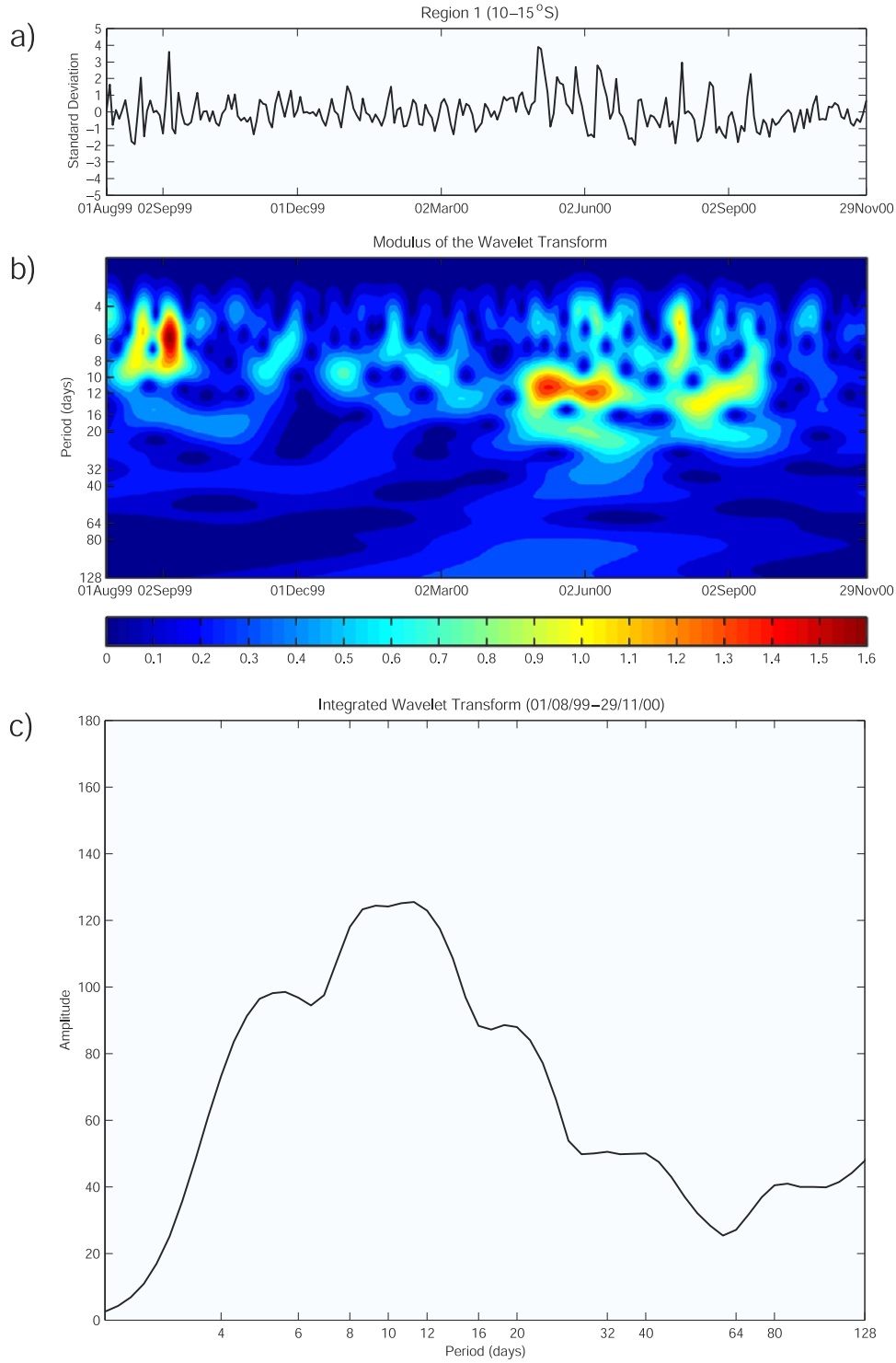

Figure 4. Region 1 (10°–15°S). (a) The standardized time series of the alongshore (v) component winds (01 August 1999 to 29 November 2000), (b) the modulus of the wavelet transform, using the Morlet wavelet, and (c) the integrated wavelet transform. The contour interval in Figure 4b is 0.1.

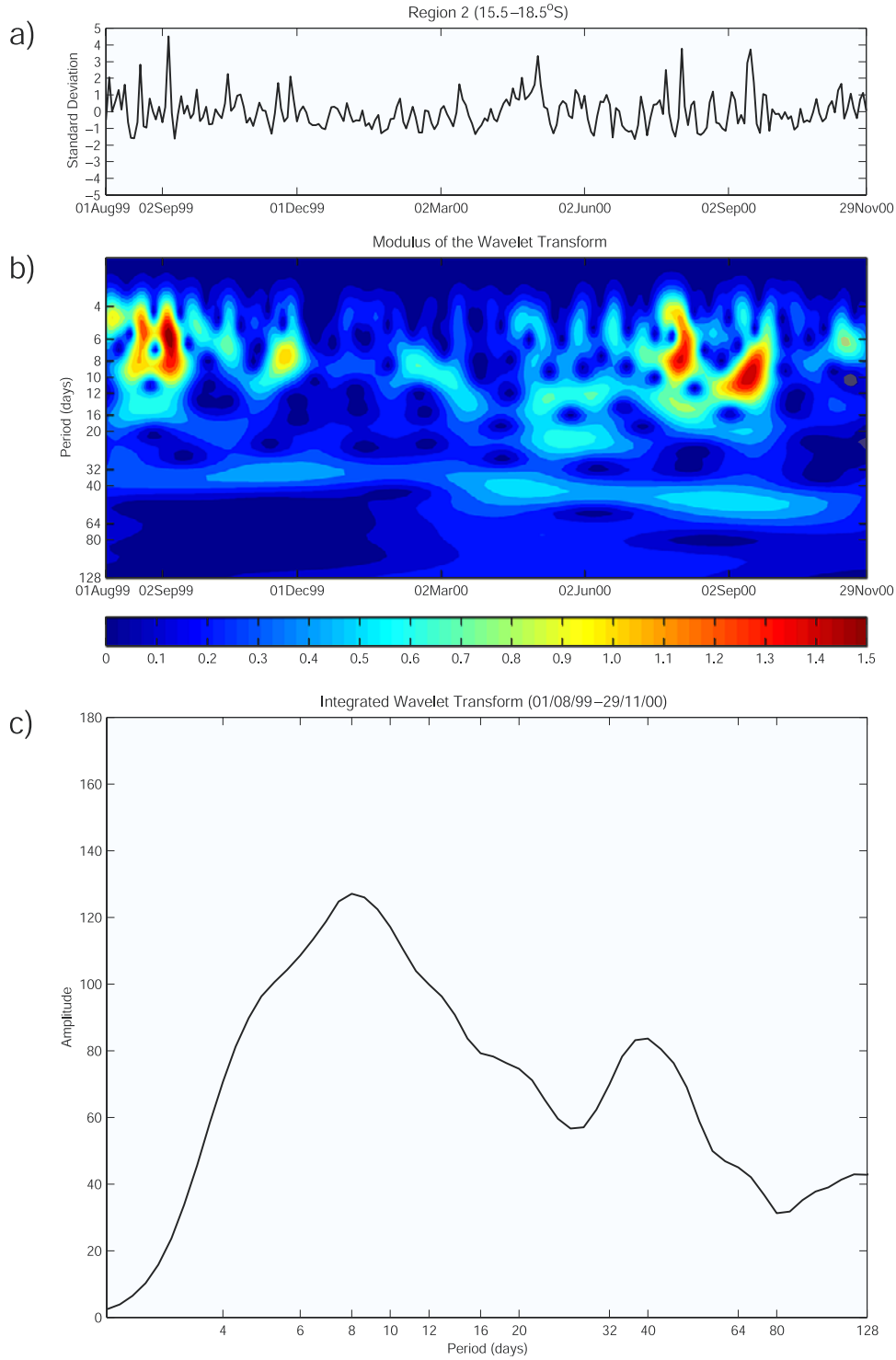

Figure 5. Region 2 (15.5°–18.5°S). (a) The standardized time series of the alongshore (v) component winds (01 August 1999 to 29 November 2000), (b) the modulus of the wavelet transform, using the Morlet wavelet, and (c) the integrated wavelet transform. The contour interval in Figure 5b is 0.1.

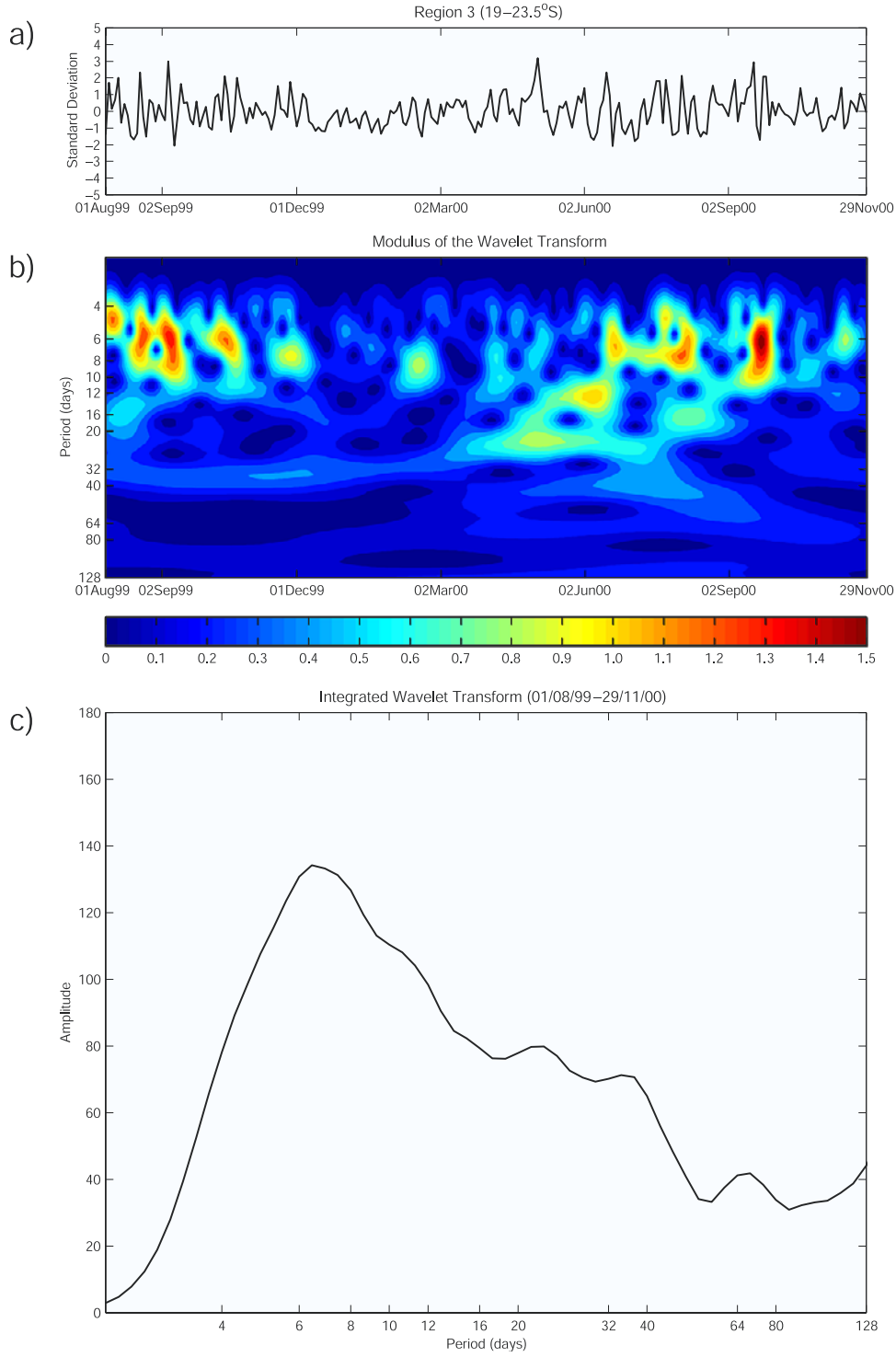

Figure 6. Region 3 (19°–23.5°S). (a) The standardized time series of the alongshore (v) component winds (01 August 1999 to 29 November 2000), (b) the modulus of the wavelet transform, using the Morlet wavelet, and (c) the integrated wavelet transform. The contour interval in Figure 6b is 0.1.

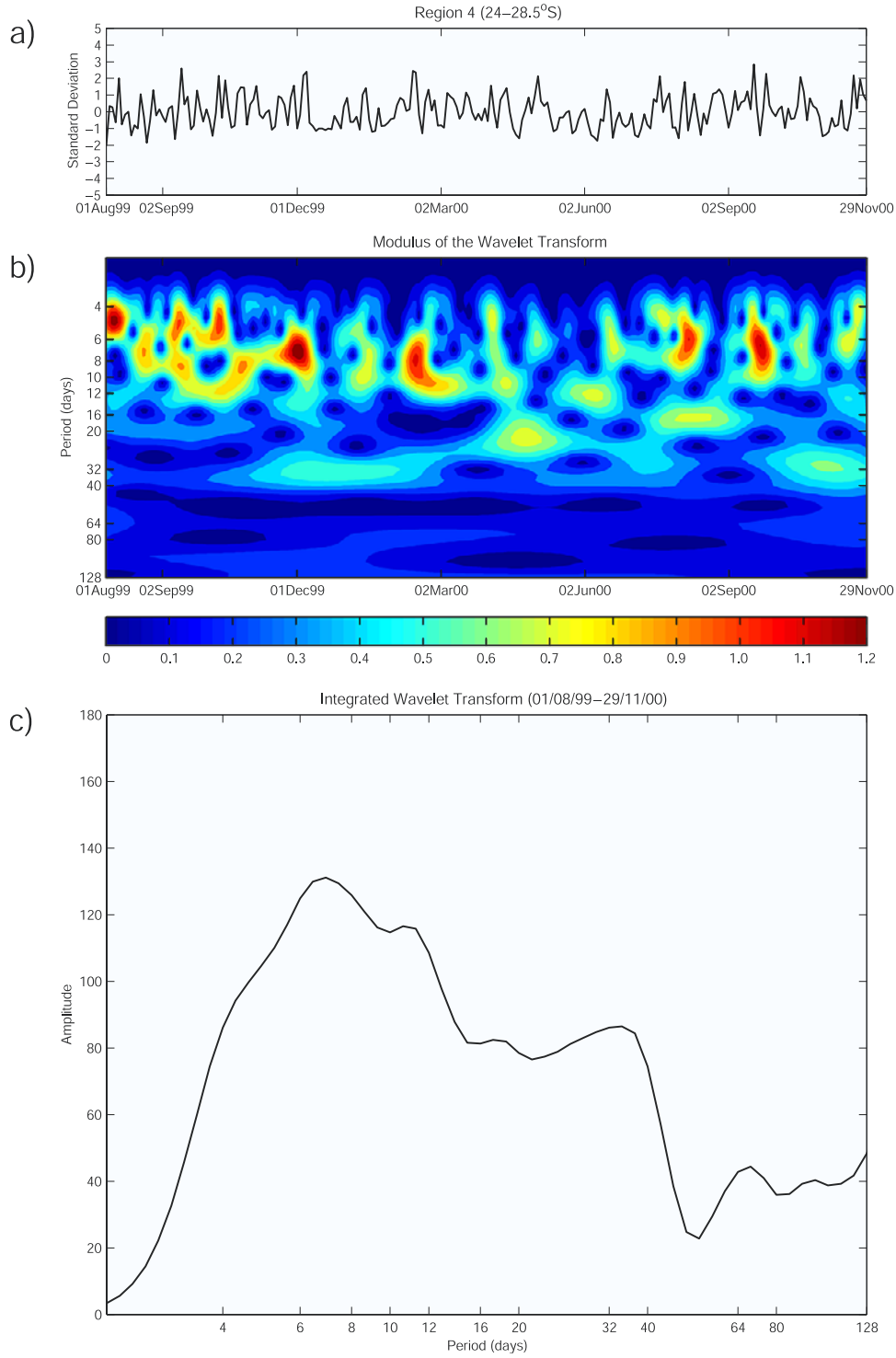

Figure 7. Region 4 (24°–28.5°S). (a) The standardized time series of the alongshore (v) component winds (01 August 1999 to 29 November 2000), (b) the modulus of the wavelet transform, using the Morlet wavelet, and (c) the integrated wavelet transform. The contour interval in Figure 7b is 0.1.

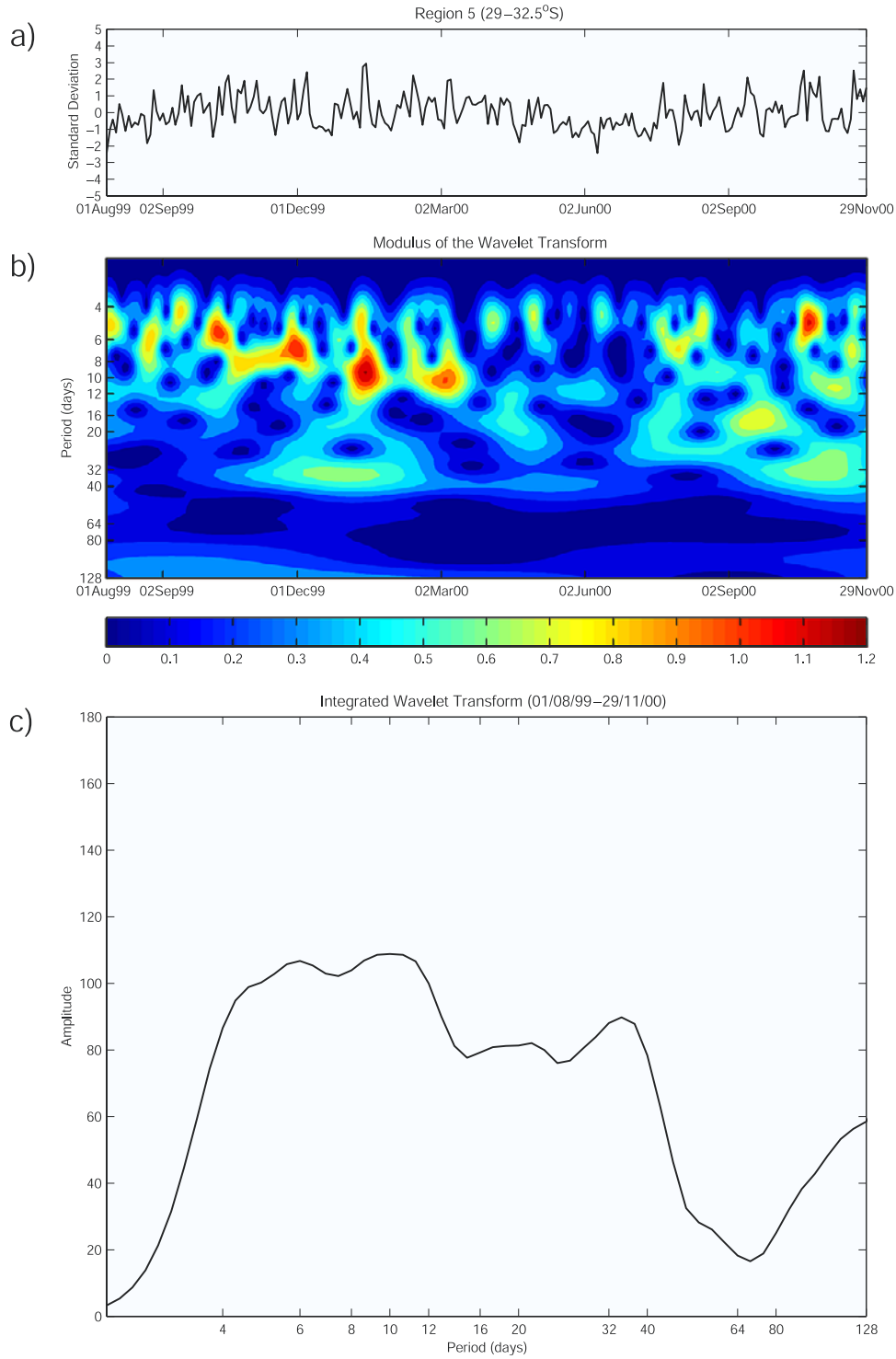

Figure 8. Region 5 (29°–32.5°S). (a) The standardized time series of the alongshore (v) component winds (01 August 1999 to 29 November 2000), (b) the modulus of the wavelet transform, using the Morlet wavelet, and (c) the integrated wavelet transform. The contour interval in Figure 8b is 0.1.

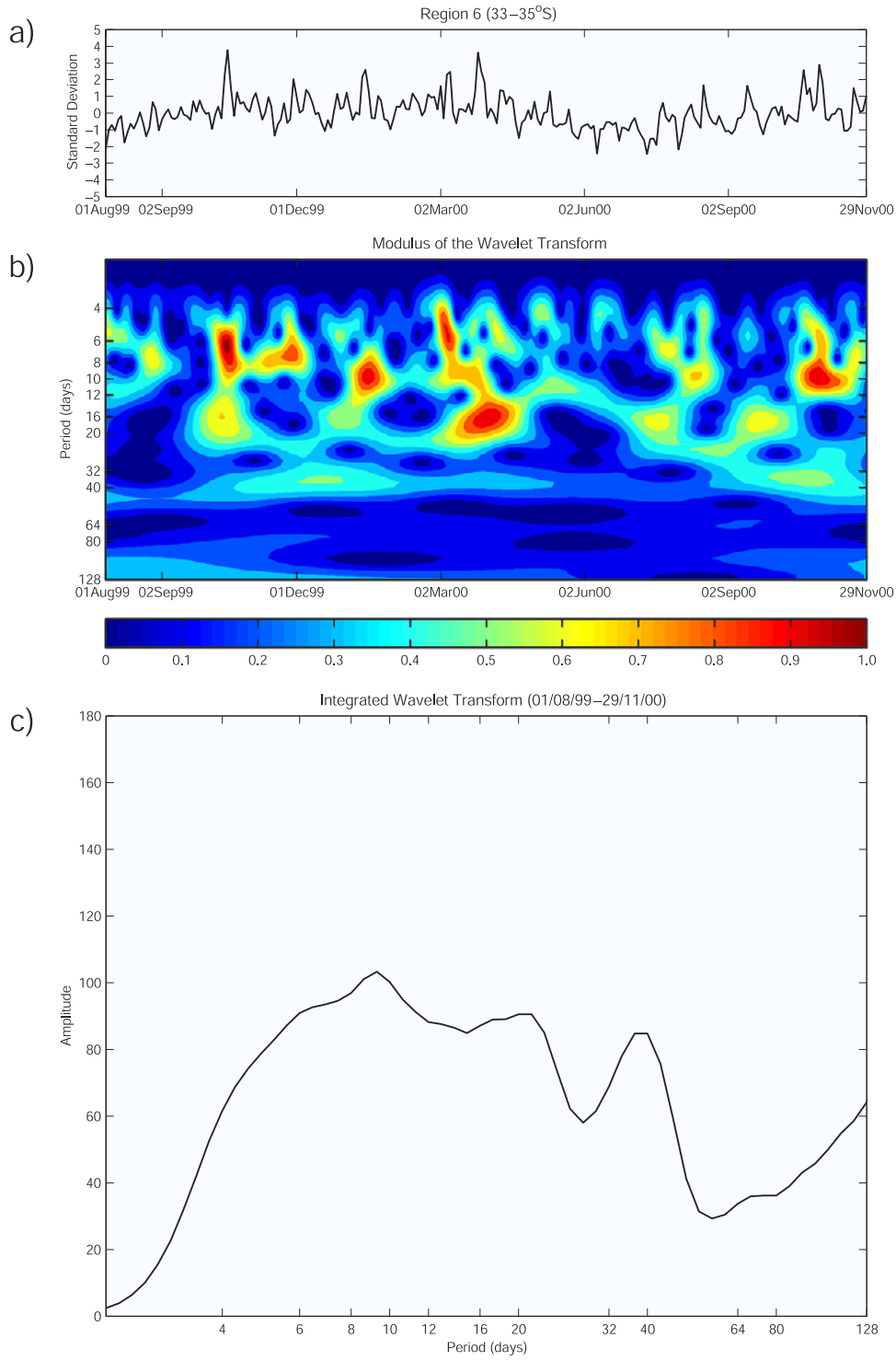

Figure 9. Region 6 (33°–35°S). (a) The standardized time series of the alongshore (v) component winds (01 August 1999 to 29 November 2000), (b) the modulus of the wavelet transform, using the Morlet wavelet, and (c) the integrated wavelet transform. The contour interval in Figure 9b is 0.1.

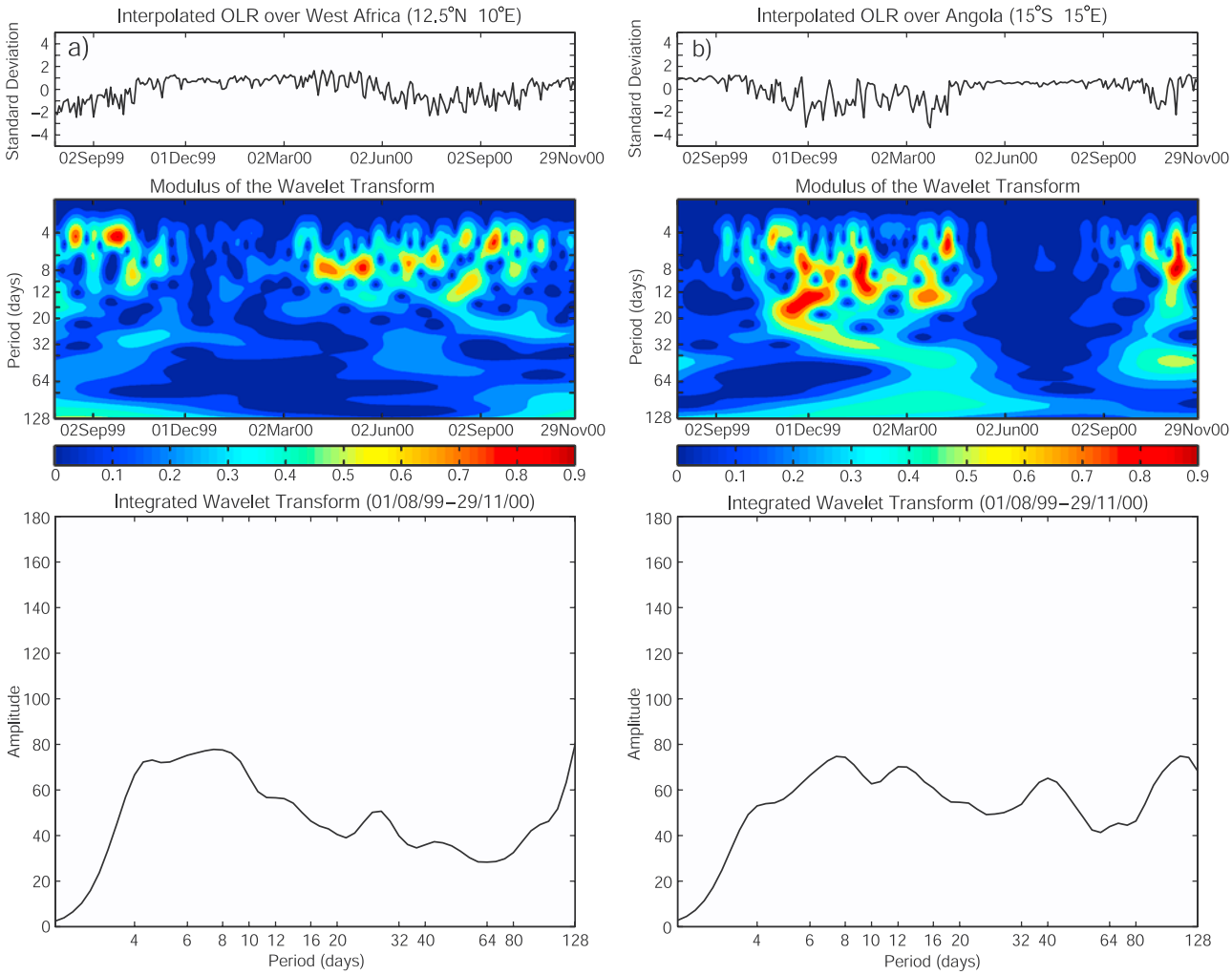

Figure 10. (a) The standardized time series of interpolated OLR data, as derived from the 2.5° resolution NCEP reanalysis data set [*Liebmann and Smith*, 1996], the modulus of the wavelet transform, using the Morlet wavelet, and the integrated wavelet transform for 12.5°N, 10°E (01 August 1999 to 29 November 2000). (b) As above but for 15°S, 15°E. The contour interval, for both Figures 10a and 10b, is 0.1.

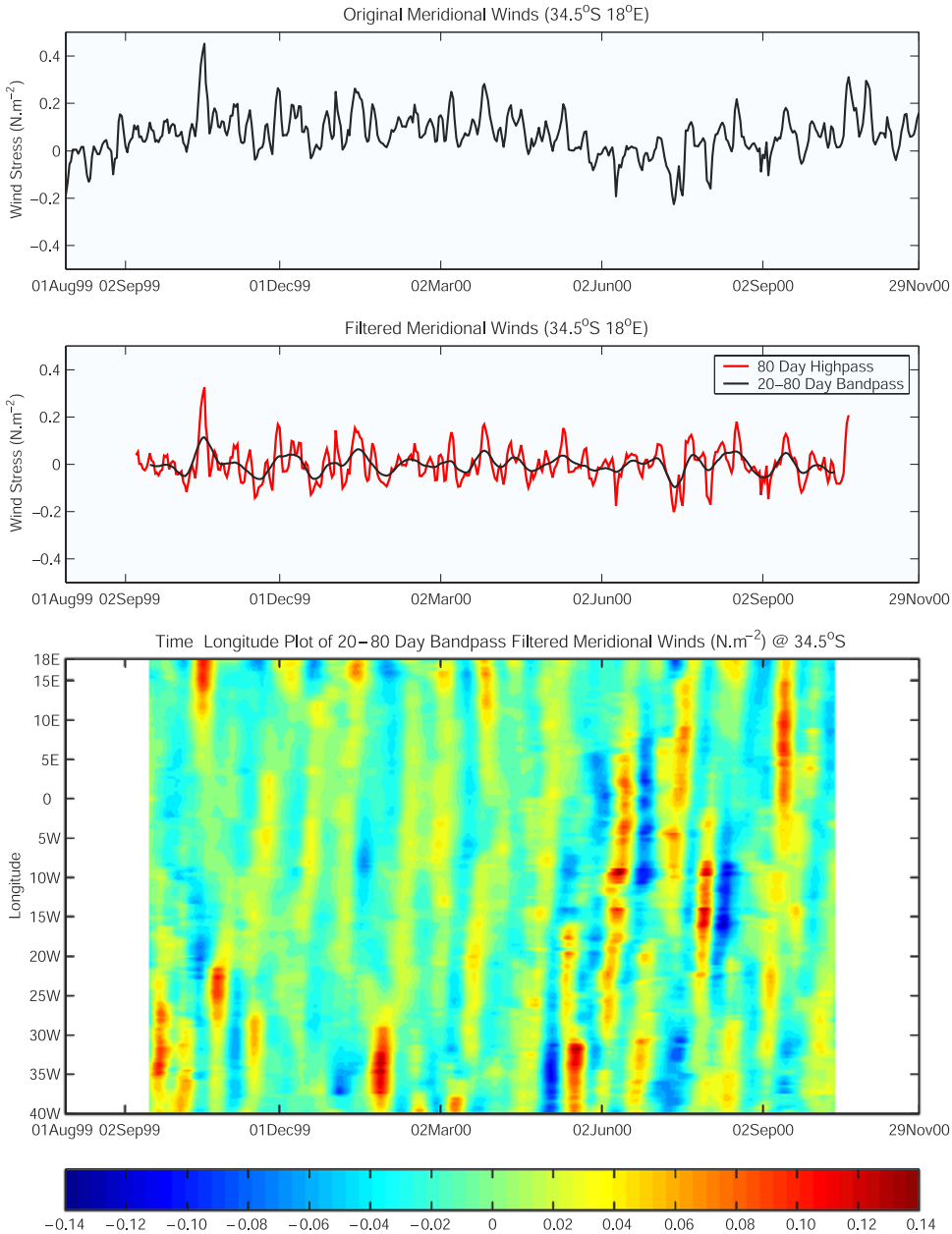

Figure 11. (top) The original QuikSCAT meridional wind stress time series (01 August 1999 to 29 November 2000) at 34.5°S, 18°E. (middle) The high-pass- (80 day) and band-pass- (20–80 day) filtered time series (10 September 1999 to 21 October 2000 and 18 September 1999 to 13 October 2000, respectively). (bottom) A time (18 September 1999 to 13 October 2000)-longitude (40°W–18°E) plot of 20–80 day band-pass-filtered meridional winds at 34.5°S. The contour interval for Figure 11 (bottom) is 0.02 N m^{-2}.